Hailfall in a Possible Future Climate Using a Pseudo–Global Warming Approach: Hail Characteristics and Mesoscale Influences

HOLLY MALLINSON,[a] SONIA LASHER-TRAPP,[a] JEFF TRAPP,[a] MATTHEW WOODS,[a] AND SOPHIE ORENDORF[a]

[a] *University of Illinois Urbana–Champaign, Urbana, Illinois*

(Manuscript received 28 March 2023, in final form 12 September 2023, accepted 30 October 2023)

ABSTRACT: Severe convective storms (SCS) and their associated hazards present significant societal risk. Understanding of how these hazards, such as hailfall, may change due to anthropogenic climate change is in its infancy. Previous methods used to investigate possible changes in SCS and their hail used climate model output and were limited by their coarse spatiotemporal resolution and less detailed representations of hail. This study instead uses an event-level pseudo–global warming (PGW) approach to simulate seven different hailstorms in their historical environments, and again in five different end-of-century PGW environments obtained from the worst-case scenario increases in CO_2 of five different CMIP5 members. Changes in large-scale environmental parameters were generally found to be consistent with prior studies, showing mostly increases in CAPE, CIN, and precipitable water, with minor changes in vertical wind shear. Nearly all simulated events had moderately stronger updrafts in the PGW environments. Only cold-season events showed an increase in hail sizes both within the storms and at the surface, whereas warm-season events exhibited a decrease in hail sizes at the surface and aloft. Changes in the event-total hailfall area at the ground also showed a seasonal trend, with increases in cold-season events and decreases in warm-season events. Melting depths increased for all PGW environments, and these increases likely contributed to greater rainfall area for warm-season events, where an increase in smaller hail aloft would be more prone to melting. The differences in PGW simulation hail sizes in cold-season and warm-season events found here are likely related to differences in microphysical processes and warrant future study.

SIGNIFICANCE STATEMENT: It is uncertain how severe thunderstorm hazards (such as hail, tornadoes, and damaging winds) may change due to human-induced climate change. Given the significant societal risk these hazards pose, this study seeks to better understand how hailstorms may change in the future. Simulated end-of-century storms in winter months showed larger hail sizes and a larger area of event-total hailfall than in the historical simulations, whereas simulated future storms in spring and summer months showed smaller hail sizes and a reduction in the area where hail fell. An analysis of traditional environmental and storm-scale properties did not reveal a clear distinction between cold-season and warm-season hailstorms, suggesting that changes in small-scale precipitation processes may be responsible.

KEYWORDS: Climate change; Hail; Mesoscale processes; Storm environments; Mesoscale models

1. Introduction

Severe convective storms (SCS) and their associated hazards (i.e., hail, damaging winds, tornadoes) present a significant societal risk, with billion-dollar events occurring nearly four times as frequently as other natural disasters and accounting for over $170 billion in damage from 2010 to 2019 in the United States (NOAA NCEI 2022). It is thus imperative to understand how these storms and their hazards may change due to anthropogenic climate change (ACC). While changes to severe thunderstorms and their environments are better understood, confidence remains low in understanding how they may translate to changes in their associated hazards due to coarse climate model resolution and the approximations necessary within parameterizations used in current climate models (IPCC 2021). Current and future trends in hailstorms due to climate change are among those difficult to evaluate, as summarized in a recent review by Raupach et al. (2021), where multiple paths forward, including improving observational databases, better evaluation of environmental proxies, process-level modeling, and additional study of economic impact and vulnerability, have all been recommended.

Observing changes in hail (and other convective weather hazards) as the climate changes is difficult due to the rarity of these events, changing reporting practices, and the relatively short dataset length (Brooks 2013; Kunkel et al. 2013; Allen and Tippett 2015). In hail observational databases, numerous studies have noted significant nonmeteorological biases, such as population bias (Cecil 2009), lack of reporting to government weather agencies (Blair and Leighton 2012), duplicate reporting and changes in the definition of severe hail size (Allen and Tippett 2015), and underestimation of reported

Supplemental information related to this paper is available at the Journals Online website: https://doi.org/10.1175/JCLI-D-23-0181.s1.

Mallinson's current affiliation: NASA Postdoctoral Program, Goddard Space Flight Center, Greenbelt, Maryland.

Woods' current affiliation: National Weather Service, Las Vegas, Nevada.

Orendorf's current affiliation: Cooperative Institute for Great Lakes Research, University of Michigan, Ann Arbor, Michigan.

Corresponding author: Holly Mallinson, hmm2@illinois.edu

DOI: 10.1175/JCLI-D-23-0181.1

hail size, especially for large hail exceeding 2 in. (5.1 cm) in diameter (Blair et al. 2017).

Regional hail climatologies have generally been produced using radar-derived hail products and/or public hail reports (e.g., Doswell et al. 2005; Cintineo et al. 2012; Ortega 2018; Janssen Schile et al. 2019) but are better suited to examining the frequency of hail-producing storms, rather than the maximum hailstone sizes at the ground. Using radar data, hail occurrence is typically detected using the derived maximum expected size of hail (MESH) product, which is a measure of vertically integrated storm reflectivity (Witt et al. 1998). Numerous studies (e.g., Edwards and Thompson 1998; Lindley and Lemon 2007; Jiang et al. 2019; Ortega 2018) have found that reflectivity and its derived fields, for example three-body scatter spikes (Lindley and Lemon 2007) and vertically integrated liquid (Edwards and Thompson 1998), provide little skill in quantifying hail size.

As a result of all these difficulties with hail observations, numerous studies (e.g., Brooks 2013; Allen and Tippett 2015; Allen et al. 2017) state that environmental parameters are better suited for studying long-term trends in hailfall related to ACC compared to observational methods. Past studies have used a combination of parameters, namely instability (CAPE) and bulk vertical wind shear (VWS), although some studies also include lapse rates (e.g., Brooks et al. 2003), surface moisture (e.g., Trapp et al. 2007), and/or surface convergence (e.g., Van Klooster and Roebber 2009) to discern changes in *general* severe convective environments from reanalysis data. Changes in convective storm frequency and strength, as well as changes in hazards, are then extrapolated.

Some studies have used coarse global or regional climate model (GCM or RCM) output to compare historical and future severe convective environments (SCEs) over the continental United States to evaluate possible trends under ACC. The SCEs are predominately discerned using a combination of CAPE and VWS. Most studies (i.e., Trapp et al. 2007; Diffenbaugh et al. 2013; Seeley and Romps 2015; Lepore et al. 2021; Haberlie et al. 2022) find an increase in the number of days with favorable SCEs in future climate scenarios, driven mainly by an increase in the number of days with sufficient CAPE (resulting from increases in boundary layer moisture), despite decreasing VWS. However, decreases in VWS may not necessarily impact convective storm formation; Trapp et al. (2007) found that CAPE increases can sufficiently overcome decreases in wind shear, Diffenbaugh et al. (2013) found that days with decreases in shear corresponded with days with low CAPE anyway, and Seeley and Romps (2015) found that variations in shear did not explain the variabilities in changes in SCEs as well as CAPE. These studies, as well as that of Van Klooster and Roebber (2009), predict a shift toward stronger convective storms in the future, given expected increases in CAPE due to warmer surface temperatures and increases in low-level moisture. Using the relationship $w_{\max} = \sqrt{(2 \times \text{CAPE})}$ [as in Holton (2004)], it is hypothesized that stronger updrafts will result in the future from the larger CAPE (Del Genio et al. 2007).

However, analysis of possible future environmental parameters to predict changes in SCEs cannot guarantee convective initiation (CI) will occur, and thus the anticipated stronger convection in future environments might never be realized despite the large CAPE. In their analyses of historical SCEs, Taszarek et al. (2021) and Pilguj et al. (2022) both found an increase in CIN as the climate has warmed, discouraging CI. In addition, CAPE is always computed for an adiabatic air parcel that ignores any entrainment of dry air. Entrainment can decrease the parcel buoyancy and may also limit the initiation of deep convection. Because GCMs and RCMs do not resolve convective storms, a direct answer to how future CIN increases may influence CI in the future cannot be addressed using this methodology.

Moreover, while environmental parameters may suggest if severe convection is possible or not, there has been limited success in predicting hailstorm occurrence or severity using storm environments alone (Allen et al. 2020). Hazards such as hailfall are not easily discerned from environmental parameters alone. Recent work by Tang et al. (2019) saw some correlation between environmental parameters and large (≥5 cm or 1.97 in.) hail *occurrence*, though there were sensitivities to the environmental variables used and the region over which the analysis was performed. Gensini et al. (2021) found machine-learning methods had better skill in predicting the probability of hail *occurrence* compared to the parameters used in Tang et al. (2019).

There is also little skill in discerning between environments to predict hail *size* at the ground, when using bulk severe weather indices calculated from environmental parameters (e.g., Edwards and Thompson 1998; Johnson and Sugden 2014; Jewell and Brimelow 2009). Machine-learning methods utilized by Gensini et al. (2021) also found limited success in distinguishing between environments producing hail with a diameter 1–2 in. (2.5–5.1 cm) versus ≥2 in. (≥5.1 cm), and mainly at very low and very high probabilities (i.e., extreme environments). Even with the use of an idealized hail trajectory model, Lin and Kumjian (2022) found that the environments with the most CAPE did not produce the largest hail sizes and noted the interplay between CAPE and VWS in modulating hail size.

To more directly investigate future changes in hail brought about by changes in environmental conditions more directly, Brimelow et al. (2017; hereafter B17) utilized environmental profiles extracted from an RCM simulation to drive the HAILCAST 1D hail growth model (Brimelow et al. 2002) and predict maximum hailstone sizes at the ground over North America for the middle of the twenty-first century. While their analysis was still limited by uncertainty as to whether or not those environmental profiles would have allowed for CI and adiabatic parcels in storm updrafts, B17 found a decrease in the frequency of small hail and an increase in the frequency of large hail. The former was due to a greater melting depth, and the latter to increases in updraft strength.

This competition between higher CAPE (acting potentially to increase hail size) and higher melting levels (acting to decrease hail size) is at the root of the uncertainty as to what the primary contributor to changes in hail size may be in a future climate. Complicating matters, an increased melting-level depth does not affect all hail sizes in the same way: smaller hail experiences more time for melting as it falls more slowly

TABLE 1. Summary of previous modeling studies focused on potential changes in hail over the United States due to ACC that include a representation of hail.

	Mahoney et al. (2012)	Brimelow et al. (2017)	Trapp et al. (2019)
Region	Colorado front range	Continental United States and Canada	Continental United States
Duration	June–August (10 largest events only)	March–September	Full year
Future period	2041–2070	2041–2070	2071–2100
Grid spacing (finest)	1.3 km	50 km	4 km
No. of GCM projections used	One	Three	One
Hail variable	Graupel/hail mass	Hail diameter obtained from HAILCAST run on environmental profiles	Column-integrated graupel/hail mass; calibrated against HAILCAST
Changes in frequency of surface hailfall	Less frequent	Less frequent	More frequent in spring, less frequent in summer
Cause of frequency changes	Increased melting depth	Increases in CIN and melting depth	Corresponds to changes in convective storm occurrence; small hail not studied
Changes in hail size at the surface	Elimination of surface hail	Shift to larger sizes for everywhere but the eastern and southeastern United States	Shift to larger sizes in summer
Causes of size changes	Increased melting depth	Increased buoyancy; offset by increased melting depth for the eastern and southeastern United States	Wider, stronger updrafts

through the warm layer. While there is consensus that the height of the 0°C isotherm will increase under ACC and result in a larger melting depth (e.g., Mahoney et al. 2012; Dessens et al. 2015; Trapp et al. 2019), Rasmussen and Heymsfield (1987), Lamb and Verlinde (2011), and Ryzhkov et al. (2013) have all noted that hail melt is also dependent upon the relative humidity (RH) profile beneath the storm through which the hail falls, with decreases in relative humidity delaying the onset of melting due to evaporative cooling of the hailstone surface. Despite some studies showing a decrease in RH under ACC (e.g., Seeley and Romps 2015; Trapp and Hoogewind 2016) no studies in the published literature have considered this effect on hail melting (e.g., instead using the 0°C wet-bulb temperature level to determine the onset of melting).

An alternative approach to analysis of environmental parameters alone is convection-permitting *dynamical downscaling*, where GCMs or RCMs are used to initialize a regional model run at much higher resolution. Convective parameterizations can thus be avoided, and instead convective storms can be explicitly represented. Convective event occurrences must be quantified using some criteria typically involving simulated radar reflectivity, updraft helicity, and/or updraft speed exceeding some given thresholds. Several studies using reanalysis data with this method have found that downscaling does reasonably well at reproducing precipitation fields (e.g., Trapp et al. 2011; Robinson et al. 2013) and reproducing SCEs connected to hazardous weather reports (e.g., Gensini and Mote 2014). Gensini and Mote (2015), Hoogewind et al. (2017), and Haberlie et al. (2022) all found increases in the frequency of SCS in the spring, supporting a lengthening of the severe weather season, with the latter two studies also noting increased SCE frequency in fall and winter in some regions of the United States. These studies also found decreasing SCS frequency in summer due to increased CIN, but storms that did form were more intense. This increased intensity sometimes extended to other seasons (Gensini and Mote 2015), but not always (Mahoney et al. 2013). More recent work by Ashley et al. (2023) found an increase in supercell frequency in late winter and early spring, and a decrease in frequency in summer, with all future storms displaying a greater intensity (based on updraft helicity). Given that supercells account for the majority of severe hail [i.e., hailstone diameter $\geq$ 2 in. (5.1 cm)] reports (e.g., Doswell et al. 2005; Blair et al. 2017), it could be reasonably expected that future increases in supercell strength might also result in larger hail sizes.

A few dynamical downscaling studies have been performed specifically to investigate hailstorm frequency and severity under climate change in the United States: Mahoney et al. 2012 (hereafter M12) and Trapp et al. 2019 (hereafter T19). T19 found a shift toward larger hail sizes over the entire United States in the future as a result of increased CAPE, whereas M12 found an increase in hail mass aloft but nearly no hail at the ground over the state of Colorado, due to an increased melting depth. T19 also noted the effects of an increased melting depth for decreases in hail frequency, but particularly an increase in CIN that decreased storm frequency in particular regions of the United States, especially the eastern region. A summary of the findings of these studies, as well as of B17, is provided in Table 1, as they indicate the current state of knowledge regarding projected hail frequency and sizes (apart from less specific SCE studies) over the United States in a future climate. Differences in grid spacing undoubtedly bring about some of the differences found among these studies, as well as how the hail was modeled (as graupel or hail mass in

single-moment parameterizations, or by a few hailstones grown in a detailed hail growth model), and how far into the future each study considered (T19 considered projections 30 years farther than M12 and B17, and thus addressed an overall warmer period).

Discrepancies in results may be at least partially due to varying methods (i.e., first six rows of Table 1), including sometimes the use of a single climate model driver, but these studies do emphasize the uncertainty caused the competing effects between higher CAPE and higher melting levels highlighted earlier. All studies saw evidence of stronger storms (for M12 this was indicated by an increase in hail mass aloft in future climate simulations) and in T19 and some regions in B17, this governs the response of hail in future climates and results in larger hail sizes. However, for M12 and the southern and eastern United States in B17, increased melting depths overruled the stronger storms and dominated the hail response, resulting in smaller hail sizes (or an elimination of surface hail for M12).

These past studies were somewhat limited in their representation of hail. M12 and T19 utilized the single-moment Thompson microphysics scheme (Thompson et al. 2008), which predicts mass for a single, combined graupel/hail category. While being computationally efficient, numerous studies have shown that double-moment schemes better represent microphysical (i.e., precipitation fields) and dynamical (i.e., storm morphology, cold pools) properties of severe convective systems better than single-moment schemes (e.g., Morrison et al. 2009; Dawson et al. 2010; Lee and Donner 2011; Van Weverberg et al. 2012; Igel et al. 2015). Due to the coarseness of their RCM simulations, B17 utilized HAILCAST, which predicts surface hail size, but it is intrinsically biased toward larger hail due to using maximum updraft speeds based on CAPE (possibly increasing the residence time of larger hail in the hail growth zone) and a limited number of hail embryos (reducing competition for available supercooled liquid water). *As such, the trade-off for longer model run times for these types of simulations means that hail processes are only crudely represented.*

Furthermore, while the downscaling methodology can more directly assess SCE changes by eliminating the need for convective parameterizations, the 4-km grid spacing or larger employed by T19, as well as many other dynamical downscaling studies (e.g., Robinson et al. 2013; Gensini and Mote 2014, 2015; Hoogewind et al. 2017; Prein et al. 2017a,b; T19; Poujol et al. 2020) have been shown to have a tendency to overestimate overall storm size and precipitation, with studies suggesting that at this resolution, updrafts are forced at a larger than natural scale (e.g., Deng and Stauffer 2006) and are less susceptible to entrainment (e.g., Bryan and Morrison 2012; Caine et al. 2013; Van Weverberg et al. 2013; Robinson et al. 2013; Roh and Satoh 2014). The computational expense associated with using finer grid spacings limits studies to small spatiotemporal scales (such as only simulating the state of Colorado, as done by M12) and/or the use of a single GCM driver, so many studies are inherently limited by a lack of robustness (Kendon et al. 2017).

A different modeling approach for assessing possible impacts of ACC upon hazardous weather is the pseudo–global warming (PGW) method (Kimura and Kitoh 2007; Sato et al. 2007; Lackmann 2013; Trapp et al. 2021), previously referred to as the surrogate warming method (Schär et al. 1996; Frei et al. 1998). With the event-level application of PGW (e.g., Trapp et al. 2021), a particular weather event that has occurred in the past is simulated at high resolution, and then resimulated within various projected future environments, to allow for *the investigation of changes at the process level* [recommended in the review of needed hail research by Raupach et al. (2021)] that are responsible for the event. This allows for multiple realizations using a variety of environmental projections from different GCMs to investigate a variety of possible responses to ACC. There has yet to be a PGW study of possible changes in hail characteristics as a result of ACC that could be used to examine the pertinent underlying microphysical and kinematic processes (and their interactions). The goal of this study is to examine how storm-scale properties such as updraft strength and melting depth influence hailfall characteristics in potential future warmer climates, helping to link past studies of hailstorm environments to more robust simulations of hailstorms forming in those environments.

2. Methods

The PGW methodology allows for an event to be simulated in its historical environment and in other environments modified by ACC to evaluate responses to ACC. In the context of this work, "events" refer to hailstorms (time scales less than a day), although other studies have used this methodology to study phenomena at the weekly (e.g., Sato et al. 2007; Lackmann 2013; Patricola and Wehner 2018) or seasonal (e.g., Rasmussen et al. 2011; Prein et al. 2017a) time scales. Historical (HIST) simulations of the actual events typically use reanalysis data as initial and boundary conditions to drive a regional model, while PGW simulations are constructed by adding, to the reanalysis data, climate perturbations representative of a mean climate change for a given month under ACC; the perturbations (also referred to as "deltas") are obtained from GCMs as described below. In this way, deltas are in (near) hydrostatic and geostrophic balance and can be linearly superposed onto the unbalanced flow associated with the historical event and preserve small-scale weather patterns (e.g., Rasmussen et al. 2011; Trapp et al. 2021). Comparing the PGW to the HIST simulation illuminates the response of hailstorms to those perturbations.

Following Trapp et al. (2021), the temperature (T) field for a PGW simulation can be described as

$$T_{\mathrm{PGW}}(x, y, z, t) = T_{\mathrm{HIST}}(x, y, z, t) + \Delta T_{\mathrm{month}}, \qquad (1)$$

where $T(x, y, z, t)$ is the atmospheric state and $\Delta T_{\mathrm{month}}$ is the climate perturbation for the month in which the historical event occurred, given by

$$\Delta T_{\mathrm{month}}(x, y, z, t) = \overline{T_{\mathrm{month}}(x,y,z,t)}\big|_{\mathrm{future}} - \overline{T_{\mathrm{month}}(x,y,z,t)}\big|_{\mathrm{past}}. \qquad (2)$$

The "month" subscript is indicative of time-averaging of the mean fields for the specified month corresponding to the

event. Overbars indicate a time average, generally performed over a 10- or 30-yr period. Studies opting for the 10-yr averaging period (e.g., Lackmann 2013, 2015; Trapp and Hoogewind 2016) note that this is long enough to allow for interannual variability but short enough to prevent the need for trend removal. This study opts for 10-yr end-of-century averaging periods, using 1990–99 and 2090–99 as the historical and future time periods, respectively. Nevertheless, Woods et al. (2023) show that the PGW response is larger across different GCM drivers for a given delta-calculation method, than across different delta-calculation methods for a given GCM driver.

Earlier studies have used a simpler form of (2) that only accounts for the 3D mean field (x, y, z). In this study (as in Trapp et al. 2021), t represents subdaily GCM output used to construct monthly averages at 0000, 0600, 1200, and 1800 UTC to create diurnally varying deltas that can account for potential changes in the diurnal cycle of temperature, humidity, and winds. Compared to time-constant deltas, Trapp et al. (2021) found that diurnally varying deltas produced modest differences in convective intensity, with an average decrease of 11% in area of intense precipitating convection (defined as the area of column-maximum reflectivity at or exceeding 55 dBZ) in their limited case study.

In addition to temperature, time averages for specific humidity, zonal and meridional winds, surface pressure, and soil temperature and moisture are first obtained using (2) from the native GCM grid, then interpolated to the reanalysis data grid before subtracting the past from future averages to construct the deltas. For all but one event, the National Centers for Environmental Prediction North American Mesoscale Forecast System analysis (NAM-ANL; 218 grid) grid (which has approximately 12-km horizontal grid spacing and 60 vertical levels) was used; the 10 August 2020 event required the use of the High-Resolution Rapid Refresh (HRRR) grid as simulations with the NAM reanalysis data did not reproduce the observed convection. The deltas are then added to the corresponding reanalysis fields and interpolated to 3-hourly intervals, which is the data ingest interval used for the initial and boundary conditions in all simulations.

Deltas are generated using CMIP5 output from the GFDL CM3 (GFDL), MIROC5 (MIROC), and NCAR CCSM4 (NCAR) models, based on previous studies showing these datasets generated a range of convective storm environments (Diffenbaugh et al. 2013; Seeley and Romps 2015; Trapp and Hoogewind 2016), as well as the IPSL-CM5A-LR (IPSL) and NorESM1-M (NORESM) models [as in Trapp et al. (2021)]. The use of a large number of GCMs (compared to the studies in Table 1) provides additional variability in deltas that can be used to better assess the possible response of hailstorms to ACC. All GCM datasets used here were conducted with representative concentration pathway (RCP) 8.5 to identify the sensitivity of hailstorms to ACC more easily.

Figure 1 shows the observed hail reports from the NOAA Storm Prediction Center's Severe Thunderstorm Event Archive plotted over the computational subdomain used for simulating each of the seven events in this study. Some of these events were major hail events; others were chosen because the simulations were readily available due to PGW studies of other severe weather hazards. These events thus encompass a range of hailfall, regions, seasons, and storm modes over the United States to evaluate trends and their generality. Tornadic supercell thunderstorms occurred on 10 February and 20 May 2013 [as in Woods et al. (2023)] as well as 19 May 2013, 8 July 2020, and 10 December 2021 which also had strong linear convection along a frontal boundary; the 10 August 2020 case produced a derecho from a mesoscale convective system (Lasher-Trapp et al. 2023). Both the 2 March 2012 and 19 May 2013 cases were major hailstorm outbreaks consisting of multiple storm modes (i.e., warm-sector supercells with upscale growth) that occurred in the spring. Although hail was not the primary hazard for most of these events, they are useful for investigating if hailfall might intensify in such events under ACC, as well as provide both winter and summer events to test the seasonality of results. Even so, five of the seven events had reports of hail at or exceeding 2.5 in. (6.4 cm) in diameter in the Midwest, southeastern, or central United States (Fig. 1). These events span a variety of hailfall report frequencies and severity, geographical regions, and seasons that can be useful for identifying possible trends in hailstorms and hailfall under ACC.

The historical (HIST) and PGW simulations were conducted with version 4.0 of the Advanced Research Core of the Weather Research and Forecasting model (WRF; Skamarock et al. 2019). All experiments use nested domains (shown in Fig. 1 in the online supplemental material), with the outer domain having 3-km grid spacing (thus eliminating the need for convective parameterization) and the inner domain having 1-km grid spacing. All analysis is conducted over the extent of the 1-km domain for each event (shown in Fig. 1 herein). All simulations use the NSSL double-moment microphysics scheme (Mansell et al. 2010); in preliminary testing, this scheme was the only double-moment scheme in the WRF Model able to simulate the 2 in. (5.1 cm) hail that was observed in the 20 May 2013 event. The inclusion of graupel and hail as separate classes, the prediction of graupel and hail density for each grid box (allowing for more accurate fall speed estimates), adjustments for excessive size sorting, and the inclusion of wet and dry hail growth processes and hail shedding make this microphysical scheme preferrable for this study. Due to the short (≤36 h) integration time, the radiation schemes were not modified to reflect future changes in greenhouse gas emissions. Future changes in land use were also not considered.

Understanding how the maximum hail size is calculated within WRF is essential for interpreting the simulation results. For double-moment microphysics schemes within WRF, the hail size distribution is represented by the modified gamma distribution:

$$N(D) = N_0 D^{\alpha} e^{-\lambda D}, \tag{3}$$

where N is the number of hailstones of diameter D, the intercept (N_0) and the slope (λ) are predicted by representation of the underlying physical mechanisms causing increases or decreases in the hailstone sizes, and the shape parameter (α) is held constant (this work uses $\alpha = 1$ throughout). Because gamma functions are continuous (and thus the maximum D is

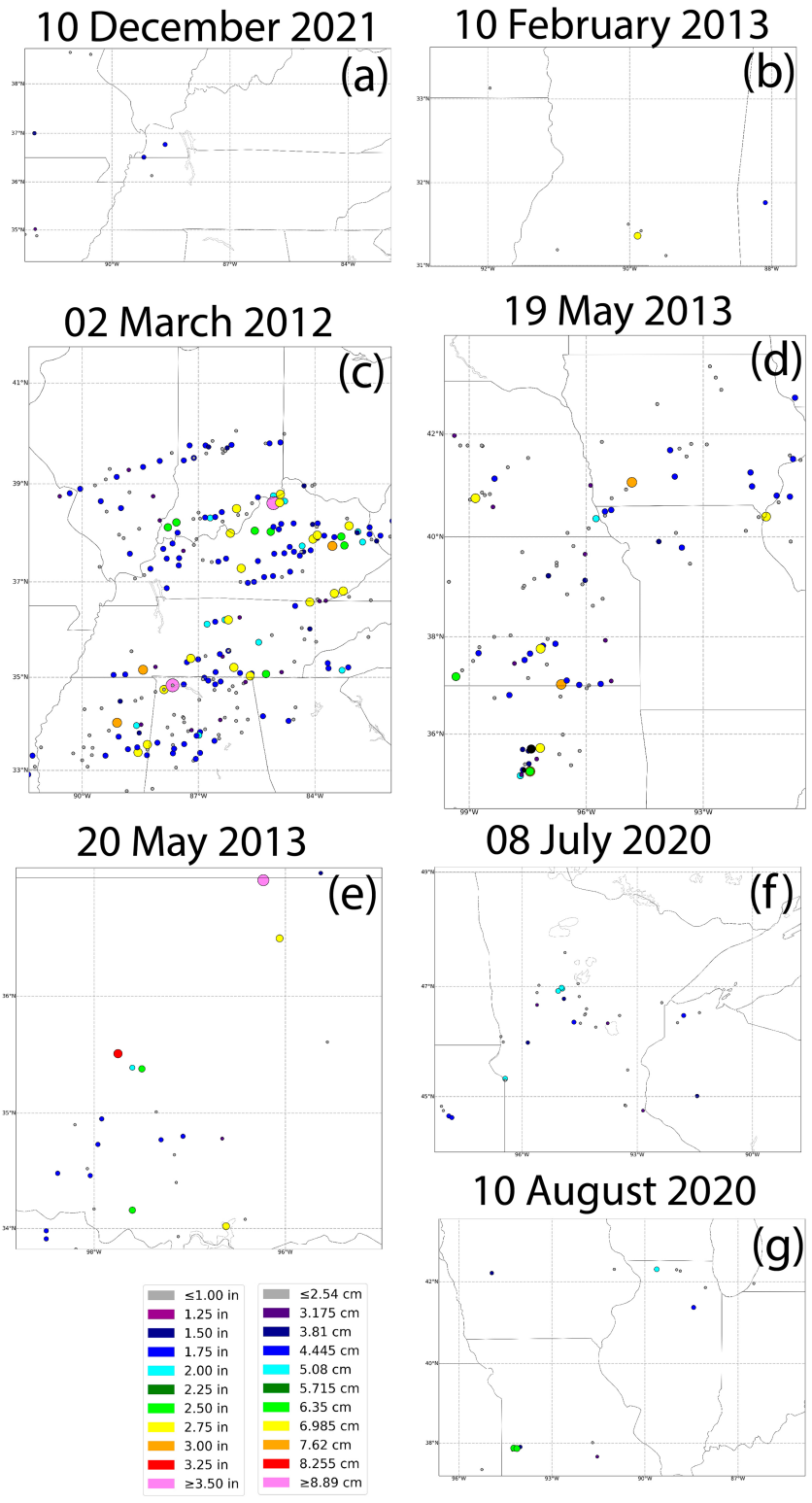

FIG. 1. Observed hail sizes and locations from the NOAA Storm Prediction Center's Severe Thunderstorm Event Archive for each of the events, plotted within the area of the innermost computational domain used in the simulations upon which the analysis is performed. The 20 May 2013 domain is zoomed in over central Oklahoma; the 8 July domain is primarily over Minnesota and northern Michigan. Dot color corresponds to hail size as indicated in legend.

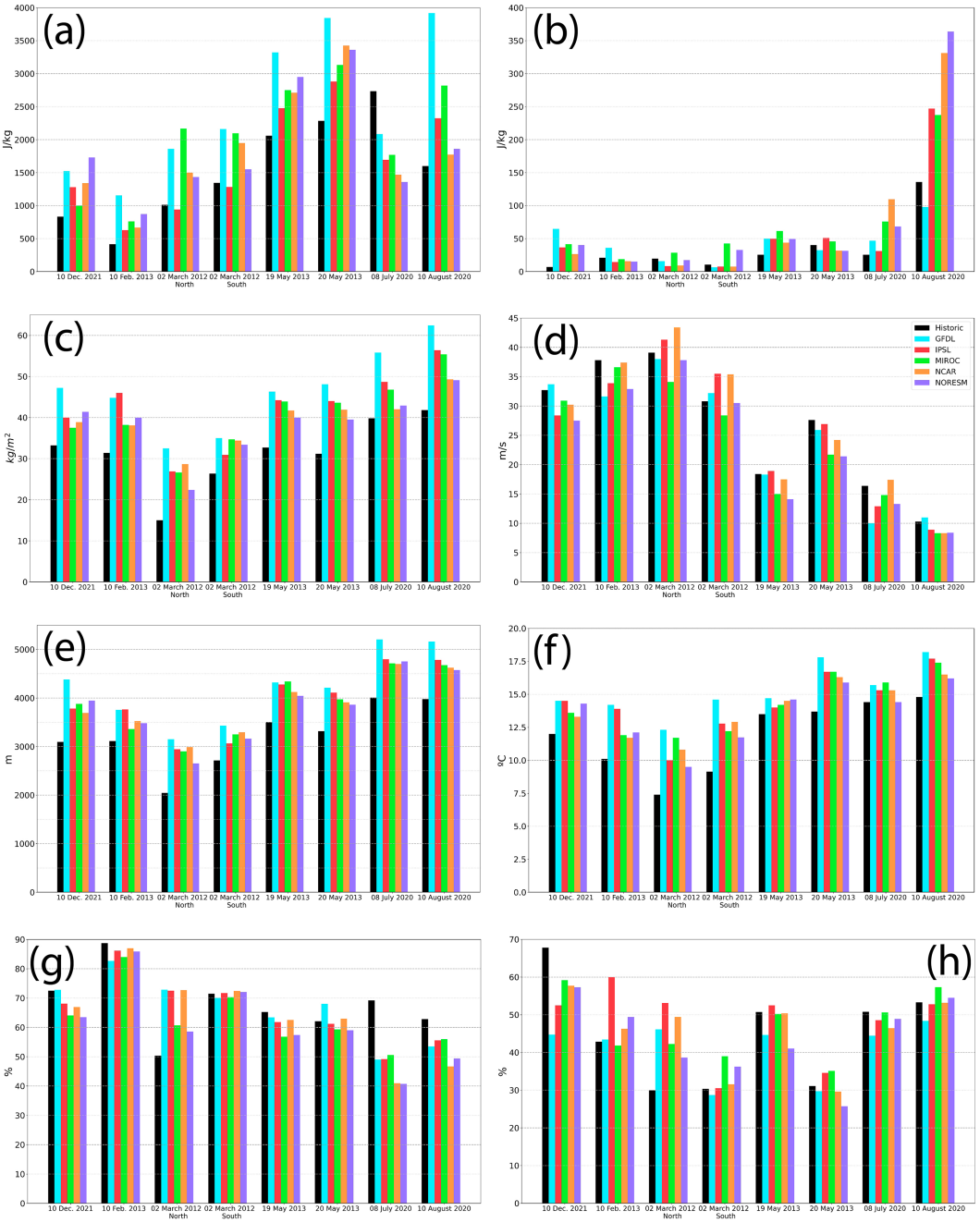

FIG. 2. Averages over domain with 1-km grid spacing at time of convective initiation of (a) CAPE, (b) CIN, (c) precipitable water (PW), (d) bulk vertical wind shear (VWS) over the 0–6-km layer, (e) melting-level height, (f) wet-bulb temperature within the melting layer for Historical and PGW cases, grouped by event, (g) relative humidity (RH) over the 900–700-hPa layer, and (h) RH over the 700–500-hPa layer. Grid columns with convection (i.e., integrated simulated reflectivity $>$ 0 dBZ) are excluded. CAPE and CIN are analogous to MUCAPE and MUCIN. WRF-Python finds the maximum θ_e in the lowest 3 km and centers a parcel with a depth of 500 m over this level. Then, temperature and moisture characteristics are averaged over the parcel depth and used in calculating CAPE and CIN.

technically infinite), a threshold is used to distinguish between hail concentrations that are considered "physically observable" and those that are not (Milbrandt and Yau 2006). The WRF Model breaks this size distribution into 50 diameter size bins, and the maximum size is determined where the upper limit of that size bin first attains a minimum number concentration threshold of 5×10^{-4} m^{-3}; i.e., one hailstone of that size over an approximately 160-m^2 area. High-resolution in situ observations

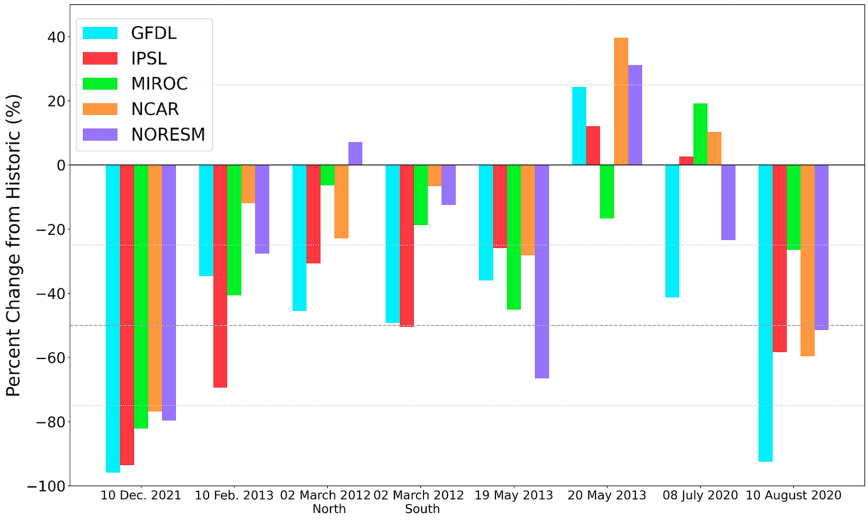

FIG. 3. Percent change in total storm area, computed as the area of a simulated column-maximum reflectivity of 25 dBZ or greater throughout the duration of the simulation between HIST and PGW simulations grouped by event.

from Blair et al. (2017) support the use of the default WRF threshold, as their high-resolution, in situ hail observations reported mode and maximum size over an area less than 200 m^2. The upper limit for the largest size bin used in WRF is 7.5 cm (2.95 in.), and thus maximum hail size is intrinsically constrained to be at or below this size. Additionally, since hail size in the WRF Model is derived via the hail mass, the assumption of spherical hailstones is prone to underestimating hail diameter, given that observed hailstones often take a more elliptical form (e.g., Knight 1986; Heymsfield et al. 2018; Shedd et al. 2021). *Thus, the WRF simulations will not necessarily reproduce the rarest (i.e., largest) hailstones that may have been observed in a particular event.*

3. Results

a. Environmental changes due to the deltas

As most previous work predicting hail changes under ACC is based upon environmental parameters, a brief comparison of the HIST and PGW environments for each event is presented to relate findings here to past studies, before analyzing the actual PGW simulations themselves. Figure 2 shows the average CAPE, CIN, precipitable water (PW), 0–6-km VWS, melting-level depths and melting temperatures, and relative humidity (RH) in the 900–700- and 700–500-hPa layers at the time of convective initiation (listed for each event in supplemental Table 1) across the 1-km grid-spacing subdomain for each event. CAPE, CIN, and PW are calculated over each grid column using WRF-Python (Ladwig 2017) and then averaged over the domain; VWS is averaged similarly but calculated using MetPy (May et al. 2022). The average melting depth is calculated as the domain average of the height above the ground where the wet-bulb temperature (T_w) first reaches 0°C; the average melting temperature is calculated as the average wet bulb temperature over this depth. Domain averages of RH are calculated over the 900–700 hPa and the 700–500-hPa layers using WRF-Python.

Generally, CAPE (Fig. 2a) values are larger at the end of the century, as commonly found in previous work studying SCEs. Future values of CAPE are sometimes larger by several hundred to 1000 J kg^{-1}, indicating that storm updrafts in the PGW simulations will likely be stronger. For the 8 July 2020 event, all the GCMs predict a decrease in CAPE at the end of the century over its small computational domain (see Fig. 1). For the MIROC, NCAR, and NORESM PGW environments, it is caused by drying (water vapor mixing ratios tend to be 1 g kg^{-1} or less compared to the HIST environment) below 850 hPa in the western part of the domain; for the GFDL and IPSL PGW environments, strong upper-level warming (i.e., temperature increases exceeding 10°C at 250 and 300 hPa) across the computational domain limited the depth of the positive parcel buoyancy contributing to CAPE.

Changes in CIN values (Fig. 2b) between the HIST and PGW environments show some seasonal dependence. During the warm season (May–August), CIN generally increases in PGW simulations, consistent with prior studies (e.g., Hoogewind et al. 2017; T19). In the cooler season CIN often has minor decreases (10 J kg^{-1} or less), although some PGW environments show small increases in CIN. The 10 December case has a consistently moderate increase in CIN across all PGW environments. Because convective initiation (CI) can be deterred by high values of CIN, these environments suggest that warm-season convection in the PGW simulations may be limited by the higher CIN values or occur later in the day as additional solar heating is needed to overcome it. In contrast, cool-season convection may be encouraged given the CIN decreases.

The average PW is larger in all the PGW environments and over all seasons, often by 10 kg m^{-2} or more. In the warmer months, PW in the PGW environments exceeds 40 kg m^{-2}, and sometimes exceeds 50 kg m^{-2} (Fig. 2c). Li et al. (2017)

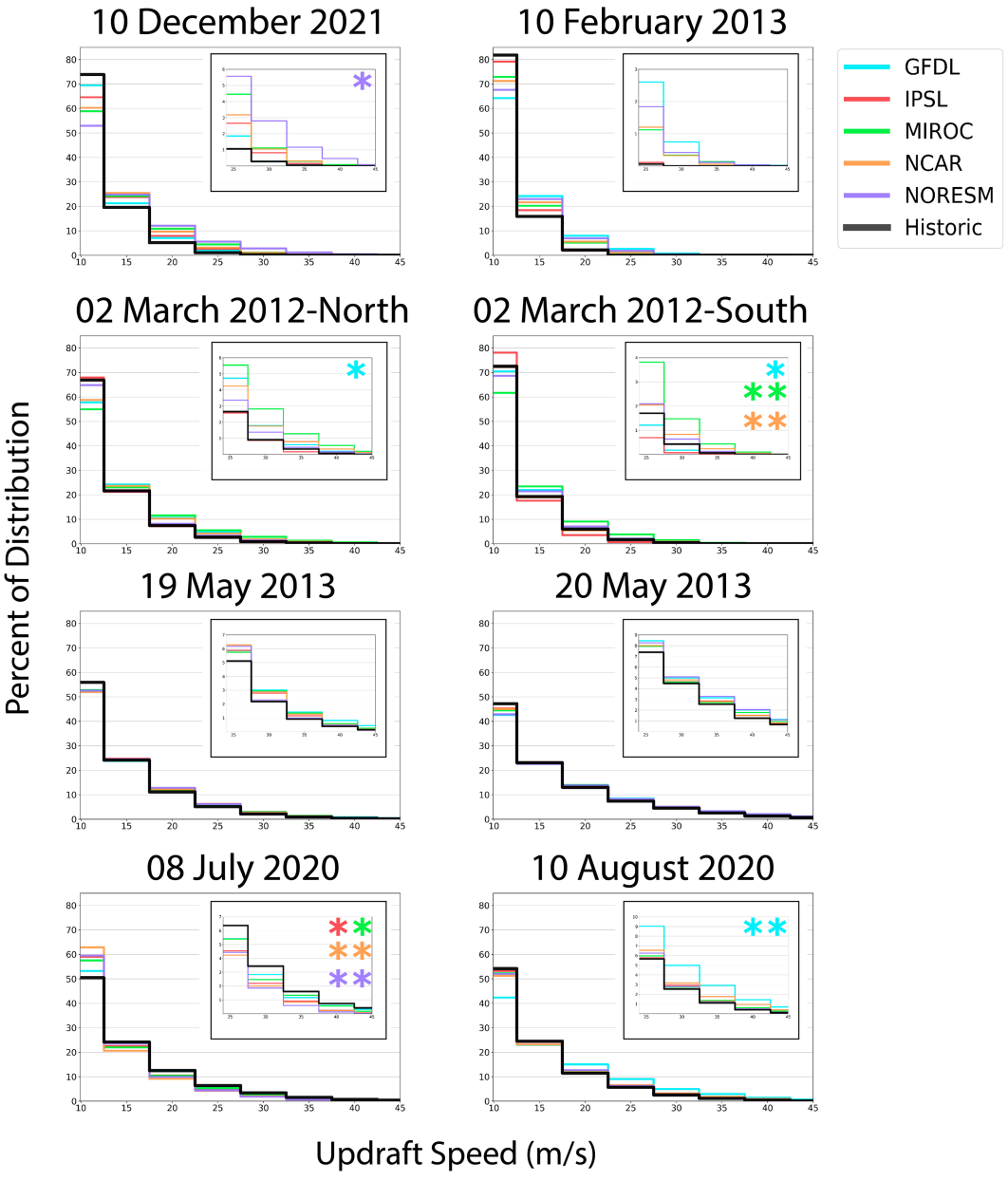

FIG. 4. Distribution of column-maximum updraft speeds 10 m s^{-1} or greater for each event taken from hourly model output. Insets for each panel zoom in on the tail of the distributions, i.e., updrafts 25 m s^{-1} and greater. Statistically significant changes at the 90% (95%) confidence interval are denoted by * (**) and are color-coded to the simulation each represents.

found that while total precipitation rate increased linearly with increasing initial moisture content, the precipitation rate of hail had a nonlinear relationship with initial moisture content, in part due to changes in cold pool characteristics that limited the development of deep convection. Thus, it is unclear how these increases in PW alone might affect hail production, further justifying using the PGW method to investigate its influence.

In contrast, the VWS is generally smaller or remains similar when comparing the PGW environments to the HIST environment, with one case (2 March 2012) suggesting some increases (Fig. 2d). In all cases, the changes in VWS tend to be small, less than 5 m s^{-1} [as also shown by Diffenbaugh et al. (2013) and Trapp and Hoogewind (2016)]. Recent idealized numerical modeling work by Dennis and Kumjian (2017) and Lin and Kumjian (2022) note the influence of VWS on hail size by altering the horizontal wind field (and thus the trajectory of hailstones through prime growth regions) that may be precluding a more direct CAPE–hail size relationship. Variations were seen in the amount of curvature to the vertical

TABLE 2. The 50th and 95th percentiles of column-maximum updraft speeds (in m s^{-1}) taken from hourly model output for HIST and PGW simulations for each event as well as the maximum to occur at any point during the simulation. Simulations where the change in the distribution of updraft speeds (as seen in Fig. 4) was significant at the 90% confidence interval are italicized; simulations with significance at the 95% confidence interval are boldface and italicized.

	Simulation	50th percentile	95th percentile	Max
10 Dec 2021	HIST	12.6	20.8	45.7
	GFDL	12.8	22.2	33.5
	IPSL	13.3	23.6	39.1
	MIROC	13.9	25.7	48.9
	NCAR	13.8	24.6	42.8
	NORESM	*14.6*	*29.3*	*55.5*
10 Feb 2013	HIST	12.2	18.4	27.2
	GFDL	13.4	23.5	49.9
	IPSL	12.3	18.5	28.3
	MIROC	12.7	21.0	38.7
	NCAR	12.9	21.2	40.5
	NORESM	13.1	22.3	45.7
02 Mar 2012–North	HIST	13.1	23.9	44.8
	GFDL	*14.0*	*27.1*	*53.4*
	IPSL	13.0	23.6	44.0
	MIROC	14.3	29.9	60.9
	NCAR	13.8	27.2	60.1
	NORESM	13.3	25.4	48.4
2 Mar 2012–South	HIST	12.6	21.9	40.4
	GFDL	*12.9*	*21.3*	*37.0*
	IPSL	12.3	19.6	33.7
	MIROC	***13.6***	***25.8***	***46.4***
	NCAR	***12.6***	***22.7***	***45.4***
	NORESM	13.0	22.9	41.6
19 May 2013	HIST	14.2	28.3	59.1
	GFDL	14.6	31.2	68.0
	IPSL	14.6	29.5	60.7
	MIROC	14.6	30.3	60.5
	NCAR	14.7	29.9	59.4
	NORESM	14.6	28.7	54.1
20 May 2013	HIST	15.5	34.8	63.4
	GFDL	16.4	39.8	77.6
	IPSL	15.8	35.7	64.2
	MIROC	16.0	36.8	68.6
	NCAR	15.8	36.7	77.0
	NORESM	16.3	38.2	76.2
8 Jul 2020	HIST	14.9	31.6	62.8
	GFDL	14.5	30.0	58.6
	IPSL	*13.8*	*27.9*	*55.2*
	MIROC	*14.0*	*29.5*	*56.7*
	NCAR	***13.4***	***27.2***	***46.3***
	NORESM	***13.7***	***26.6***	***47.9***
10 Aug 2020	HIST	14.4	29.0	53.7
	GFDL	***16.3***	***35.7***	***63.9***
	IPSL	14.5	29.9	66.4
	MIROC	14.7	30.4	68.5
	NCAR	14.8	31.9	62.1
	NORESM	14.7	29.6	67.1

profiles (i.e., hodographs) of environmental wind in addition to the covariations in CAPE and VWS. Thus, there is some uncertainty as to how changes in VWS seen here may influence hail size.

Among all GCM projections, there is unanimous agreement toward increasing melting depths in the future for all events (Fig. 2e), with increases of generally 15%–20% but sometimes over 50% compared to the HIST environment. Most notable are the increases for the northern subdomain for the 2 March 2012 event, for which the projections of melting depth were 30% to nearly 55% greater (for this reason, further analysis of the 2 March event will be conducted by dividing its computational domain into northern and southern regions). Moreover, average wet-bulb temperatures within those depths are always greater in the PGW environments, typically by several degrees (Fig. 2f). Given the increased depth for hail to melt, and the higher temperatures in this layer, one might expect small hail to become less frequent in the PGW simulations (as seen in M12).

Changes in the average 900–700-hPa environmental RH generally shows PGW environments having decreases of 10% or less relative to HIST (Fig. 2g), with the largest decreases seen for the July and August events. The northern subdomain for the 2 March 2012 event shows PGW environments with increases in RH of 10% or greater compared to HIST, attributed to stronger moisture advection in the PGW simulations (stronger southerly winds bringing enhanced moisture from the Gulf region northward) in those cases. Decreases in RH in the PGW environments may lead to increases in the effects of entrainment in these storms. The introduction of dry air induces latent cooling via enhanced evaporation/sublimation that can then decrease buoyancy (limiting updraft strength) and/or prevent CI (e.g., Morrison et al. 2020a; Peters et al. 2023). The 700–500-hPa RH increases in PGW environments for nearly all events, with cold-season PGW events having slightly greater increases compared to warm-season events. Jo and Lasher-Trapp (2023) found entrainment rates of supercells to be insensitive to environmental humidity in the midlevels, but increases in midlevel humidity were shown to increase vertical mass flux and surface rainfall. Based on the differences in environmental RH shown in Fig. 2, it could be hypothesized that future PGW storms may have weaker updrafts than anticipated by parcel theory (resulting from decreases in 900–700-hPa RH), or in other cases result in greater surface rainfall (based on the increases in 700–500-hPa RH).

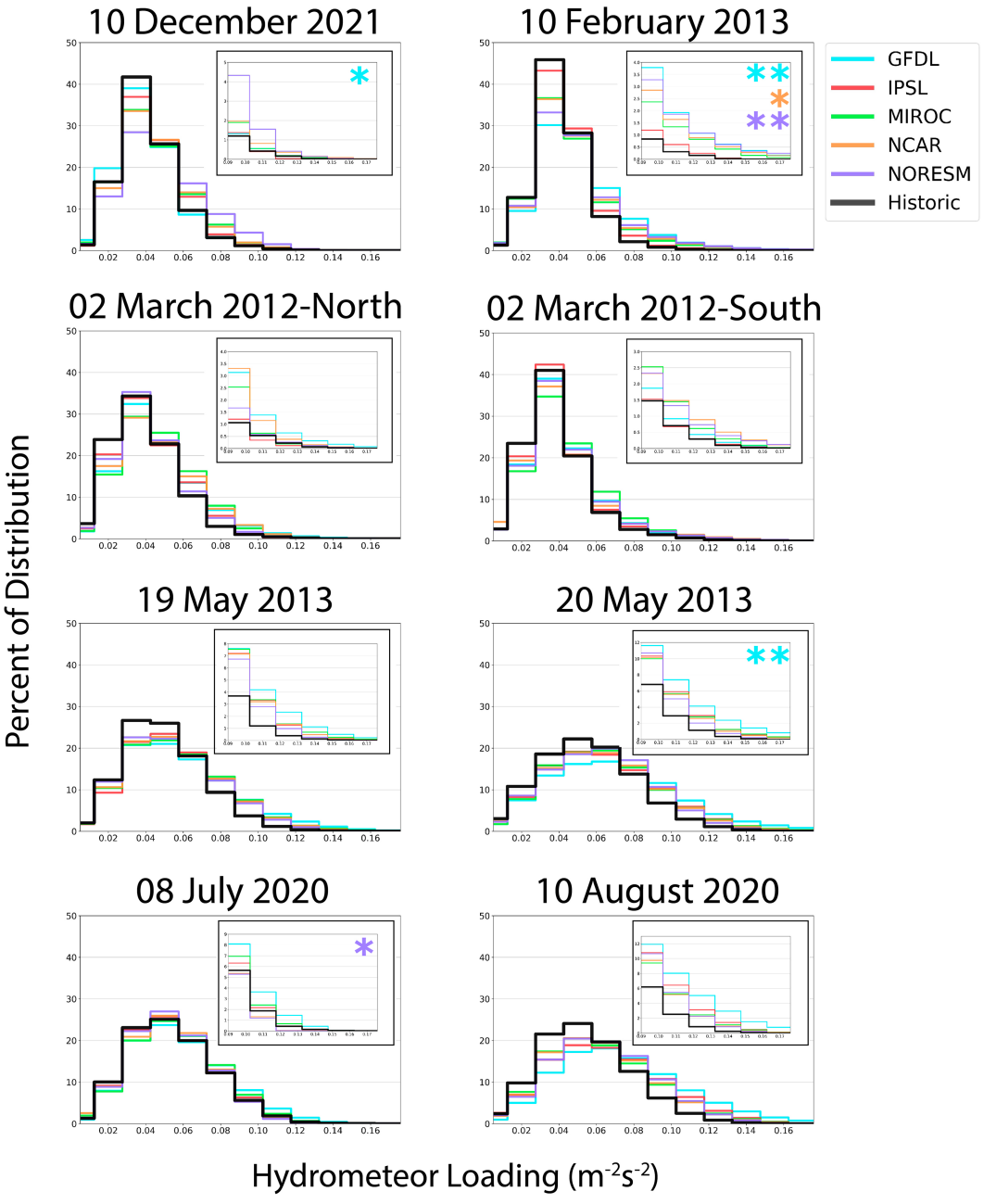

FIG. 5. Distribution of hydrometeor loading ($m^{-2}s^{-2}$) in all updrafts shown in Fig. 4. Insets in each panel zoom in on the tail of the distribution, for values of hydrometeor loading 0.1 and greater. Statistically significant changes at the 90% (95%) confidence interval are denoted by * (**).

Overall, these environmental changes generally do not differ from previous SCE studies [as summarized in Raupach et al. (2021)] and are also consistent with the findings from the studies of M12, B17, and T19 that were summarized in Table 1: larger CAPE could support stronger updrafts and potentially larger hail, although the updraft speeds could in some cases be limited by enhanced entrainment effects due to lower environmental RH. Enhanced melting may reduce or eliminate smaller hail due to greater melting depths and enhanced CIN in some cases could limit convection altogether. Thus, the working hypothesis remains that the PGW storms will have stronger updrafts, and thereby larger hail (at least within the storms), but smaller hail will be reduced due to enhanced melting. In the following sections, this hypothesis is evaluated by comparing the results from the HIST and PGW simulations from each of the seven hailstorm events (described in section 2).

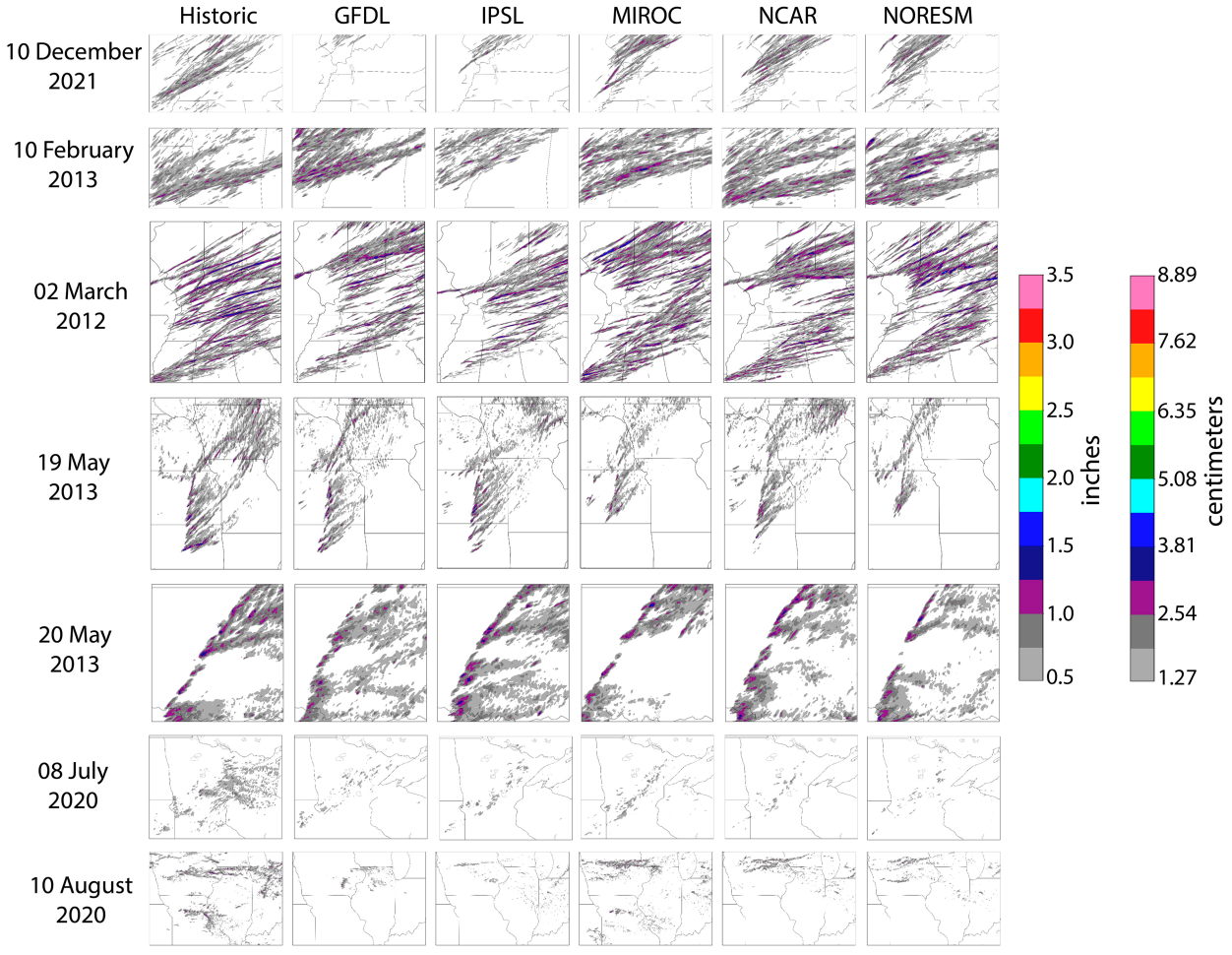

FIG. 6. Maximum hail size at the surface over the domain with 1-km grid spacing, for all simulations performed for each event. Only hail with a diameter of 0.5-in. (1.3 cm) or larger is considered.

b. *Changes between the HIST and PGW simulations*

1) TOTAL STORM AREA

Total storm area was computed as the horizontal area, throughout the duration of the simulation, of simulated column-maximum reflectivity 25 dBZ or greater. Decreases in PGW storm area are seen for nearly all events (Fig. 3) and can be attributed in part to increases in CIN (Fig. 2b), which result in the initiation of fewer storms in PGW simulations, and may also be partly due to enhanced entrainment effects resulting from the decrease in 900–700-hPa environmental RH. The delay in CI for PGW simulations (supplemental Table 1), which may also be an effect of entraining lower RH environmental air, also decreases their total storm areas relative to HIST (supplemental Fig. 2). The increases in PGW storm area seen for the 20 May 2013 event are likely due to minimal increases (or decreases) in CIN (Fig. 2b) and to much larger CAPE (Fig. 2a) in the PGW environments, resulting in larger storms. Increases in storm area for some of the PGW simulations of the 8 July 2020 event may be due to the earlier CI time seen for the PGW simulations (supplemental Table 1). While a detailed quantitative analysis of storm morphology for all simulations was beyond the scope of this study, there was no obvious shift in convective mode between PGW and HIST simulations for any event at the model resolution used here.

2) STORM INTENSITY

The distributions of storm updraft speeds ($\geq$10 m s^{-1}) in all HIST and PGW simulations for each event (Fig. 4) were used as a measure of possible changes in storm intensity due to ACC; all events except one (8 July 2020) had some PGW storms that were stronger than the corresponding HIST storms. The decreases seen in PGW updraft strengths for 8 July 2020 are attributed to the decreases in CAPE for those PGW environments (Fig. 2a). Over half of the events showed at least one PGW simulation with statistically significant increases relative to HIST (at either the 90% or 95% confidence interval) using a one-sided Mann–Whitney U test [as in Gensini and Mote (2015) and B17]. The biggest shift in the distribution of updraft speeds was the decrease in the number of weaker (10 m s^{-1}) updrafts, with PGW storms having

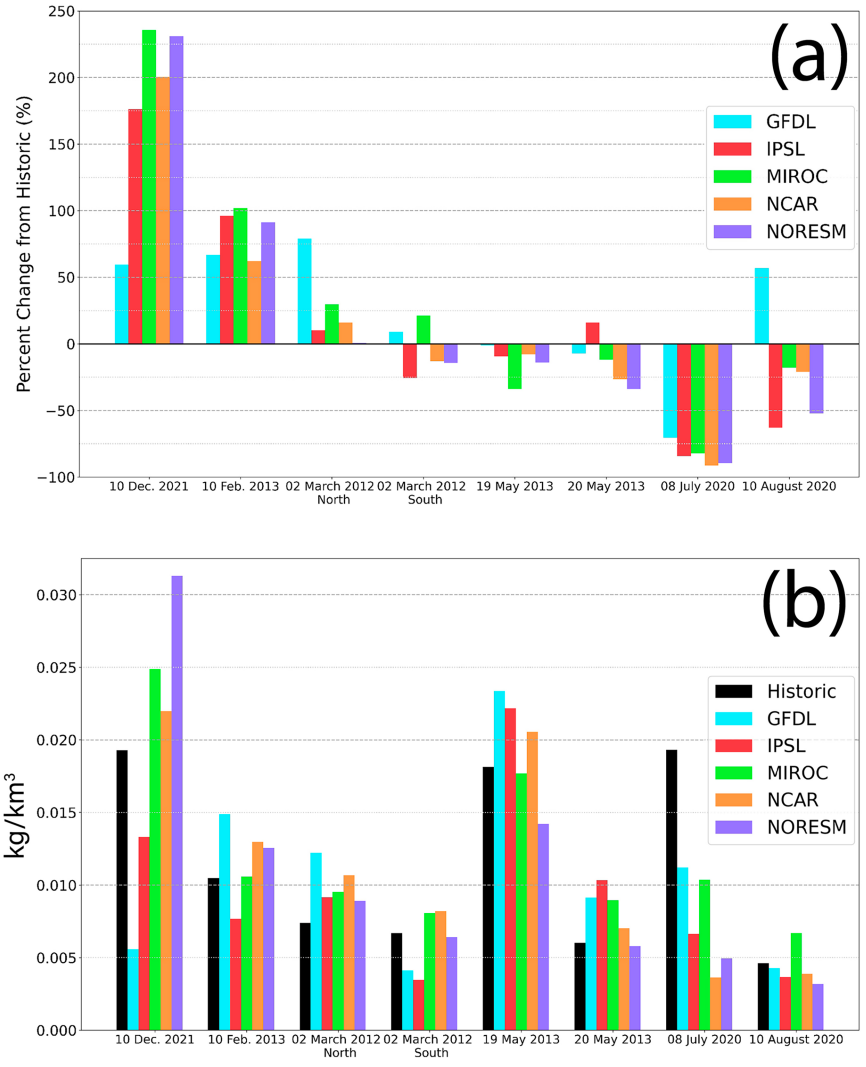

FIG. 7. (a) Percent change in total hailfall area, normalized by total storm area, between the Historical and PGW simulations for each event and (b) hail mass in updrafts ($\geq$0 m s^{-1}) taken from hourly output normalized by the updraft volume. Cold-season events are shown to the left, with progression to warm-season events as one moves to the right.

approximately 15% fewer (except 8 July). From there, slight increases in the number of updrafts with speeds 15 m s^{-1} or greater are seen, with only a 5% difference at most in the number of updrafts with speeds $\geq$ 25 m s^{-1} between HIST and PGW simulations (Fig. 4 insets).

The increase in updraft speeds in some PGW storms concurs with general increases in CAPE; however, the lack of a statistically significant increase in most PGW storms is somewhat surprising. Increases in median column-maximum updraft speeds between HIST and PGW simulations are 2 m s^{-1} or less for all simulations, with many only seeing increases of less than 1 m s^{-1} (Table 2). In fact, increases in the 95th percentile column-maximum updraft speeds typically are less than 5 m s^{-1} between HIST and PGW simulations. There is also no evidence that cold-season events consistently have larger increases in updraft speeds than warm-season events. Increases in the maximum updraft speeds throughout the simulation between HIST and PGW storms present a more robust response [as in Woods et al. (2023)], although in many cases these are well weaker than what would be expected from the CAPE values seen in Fig. 2a and using the theoretical relationship $w_{\max} = \sqrt{(2 \times \mathrm{CAPE})}$.

Modulating factors that can obscure a direct CAPE–updraft strength relationship include an increase in hydrometeor loading in the updrafts and/or entrainment, as suggested by Trapp and Hoogewind (2016). The additional PW in the PGW storm environments (Fig. 2c) can potentially be converted into more hydrometeor mass within the updraft, reducing its buoyancy and thus strength. There is indeed greater hydrometeor loading [calculated as $-gq_T$, where q_T is the total hydrometeor mixing ratio (cloud water, cloud ice, rain, graupel, hail); as in Trapp and Hoogewind (2016)] in the

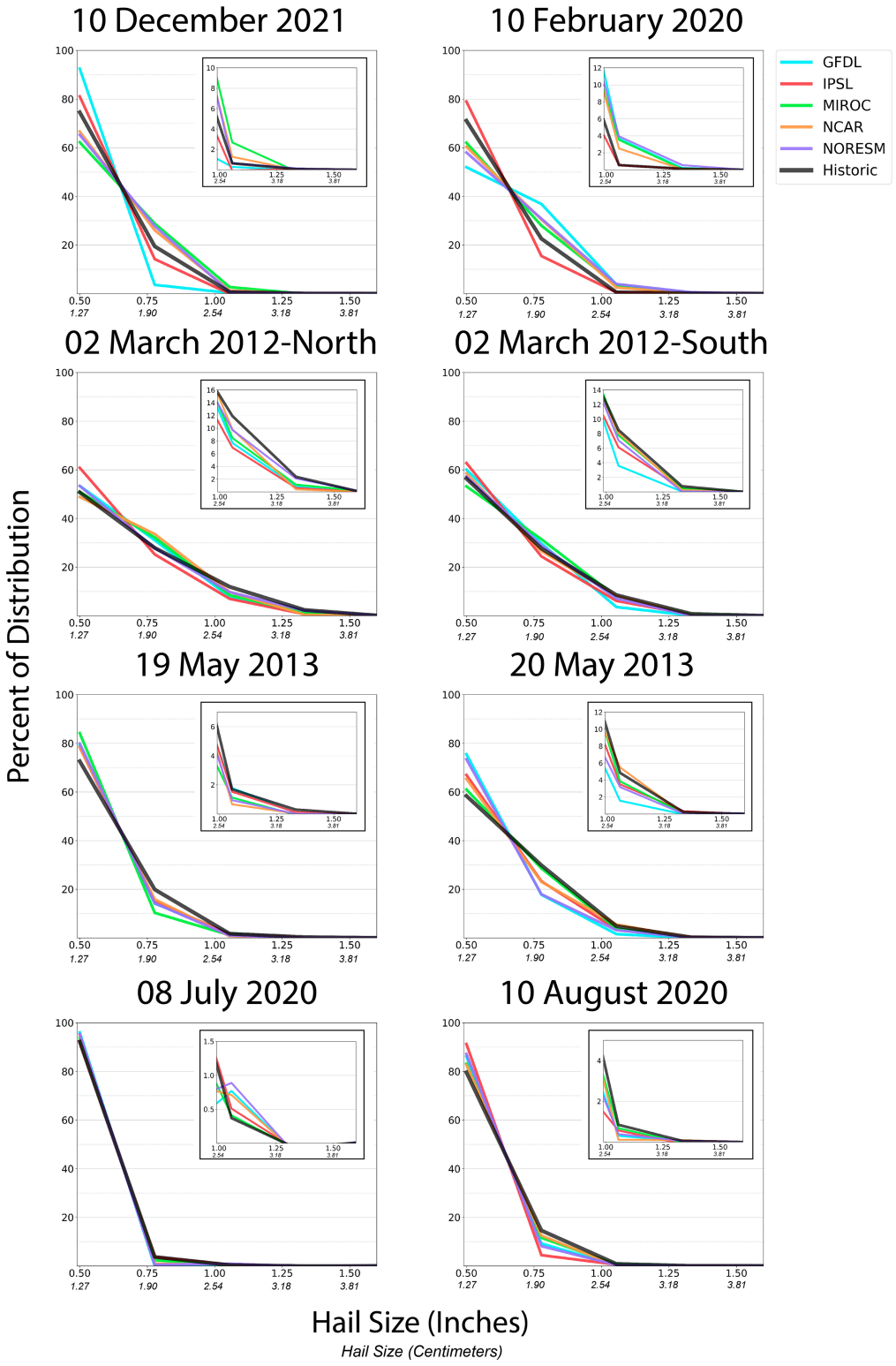

FIG. 8. Distribution of maximum hail sizes at the ground for each event, over the entire 1-km domain. Insets in each event show the distribution for hail diameters 1.0 in. (2.5 cm) and greater. There were no statistically significant changes for any events.

PGW storm updrafts (Fig. 5). A consistent signal is seen for PGW storms across all events, with decreases in the frequency of hydrometeor loading $\leq 0.06\ m^{-2}\ s^{-2}$ and an increase in the occurrence of hydrometeor loading $\geq 0.06\ m^{-2}\ s^{-2}$. However, recent numerical modeling studies (e.g., Grabowski and Morrison 2020) have shown that the reduction in buoyancy due to precipitation loading in deep convective updrafts is often offset by the gain in buoyancy due to the release of additional latent heating of freezing from that precipitation at higher levels in the storm (as long as the precipitation has not fallen out). Another possible reduction in updraft speed may also result from the entrainment of drier environmental air as shown in Fig. 2g. Thus, contrary to the original hypothesis that greater CAPE due to ACC will lead to stronger updrafts and thus potentially larger hail, one might now expect that the production of much larger hailstones may not be universal in these PGW storms, because the storm updrafts are not always stronger, and rarely substantially stronger (Table 2). This possibility is explored in subsequent sections of this study.

3) HAILFALL AREA AND SIZES

Total hailfall area for each simulation was computed as the sum of all individual hailfall swaths at the ground where hail size was 0.5 in. (1.27 cm) or larger (supplied by the WRF output variable "HAIL_MAXK1") over the duration of the simulation (Fig. 6). Comparing the total hailfall areas between the HIST and PGW storms for each event, changes are (unsurprisingly) consistent with changes in total storm area in the PGW simulations (Fig. 3). When the total hailfall area is normalized by the total storm area for each simulation (Fig. 7a), a seasonal trend emerges, with cold-season events (December and February and the northern part of the domain in the March case) showing an increase in event-total hailfall area for a given amount of event-total storm area, and warm-season events (July and August) generally showing decreases. For the cold-season events, much more integrated hail mass is being created within their updrafts for at least some of the PGW simulations compared to the respective HIST simulations (Fig. 7b). Smaller increases, or even decreases, in the hail in the PGW storm updrafts relative to the HIST simulations occur in the warm season events (July and August; Fig. 7b).

A seasonal trend is also seen in the WRF-diagnosed maximum hail sizes at the ground [supplied by the WRF output variable "HAIL_MAXK1"; see discussion of Eq. (3) in section 2] in the PGW simulations (Fig. 8). The cold-season events (December and February) generally show increases in the occurrence of the largest hail sizes in the distribution, but no trend toward the overall maximum sizes increasing substantially. For all other events, the distributions of maximum hailstone sizes at the ground shift toward smaller sizes, except for the 8 July 2020 case (in that case the increase in hail at the largest sizes might be an artifact of quantifying the far tail of the distribution in that case). None of these changes are statistically significant (based on a one-sided Mann–Whitney U test), given that the difference in maximum hail sizes at the ground between the HIST and PGW simulations is relatively minimal. For example,

TABLE 3. The 50th and 95th percentiles of maximum hail size (in inches 1 in. = 2.54 cm) at the surface for HIST and PGW simulations for each event.

	Simulation	50th percentile	95th percentile
10 Dec 2021	HIST	0.56	0.89
	GFDL	0.51	0.74
	IPSL	0.55	0.85
	MIROC	0.63	0.99
	NCAR	0.60	0.94
	NORESM	0.63	0.94
10 Feb 2013	HIST	0.59	0.91
	GFDL	0.71	1.02
	IPSL	0.58	0.87
	MIROC	0.66	1.01
	NCAR	0.65	0.99
	NORESM	0.67	1.03
2 Mar 2012–North	HIST	0.67	1.21
	GFDL	0.67	1.11
	IPSL	0.61	1.07
	MIROC	0.69	1.13
	NCAR	0.70	1.13
	NORESM	0.64	1.18
2 Mar 2012–South	HIST	0.64	1.11
	GFDL	0.65	1.01
	IPSL	0.57	1.03
	MIROC	0.67	1.10
	NCAR	0.63	1.10
	NORESM	0.64	1.07
19 May 2013	HIST	0.55	0.91
	GFDL	0.53	0.88
	IPSL	0.52	0.87
	MIROC	0.51	0.81
	NCAR	0.53	0.84
	NORESM	0.54	0.85
20 May 2013	HIST	0.63	1.02
	GFDL	0.57	0.92
	IPSL	0.62	1.00
	MIROC	0.65	1.01
	NCAR	0.59	1.02
	NORESM	0.56	0.94
8 Jul 2020	HIST	0.51	0.74
	GFDL	0.48	0.68
	IPSL	0.48	0.72
	MIROC	0.46	0.69
	NCAR	0.46	0.68
	NORESM	0.45	0.66
10 Aug 2020	HIST	0.53	0.84
	GFDL	0.52	0.80
	IPSL	0.49	0.73
	MIROC	0.51	0.82
	NCAR	0.51	0.82
	NORESM	0.49	0.76

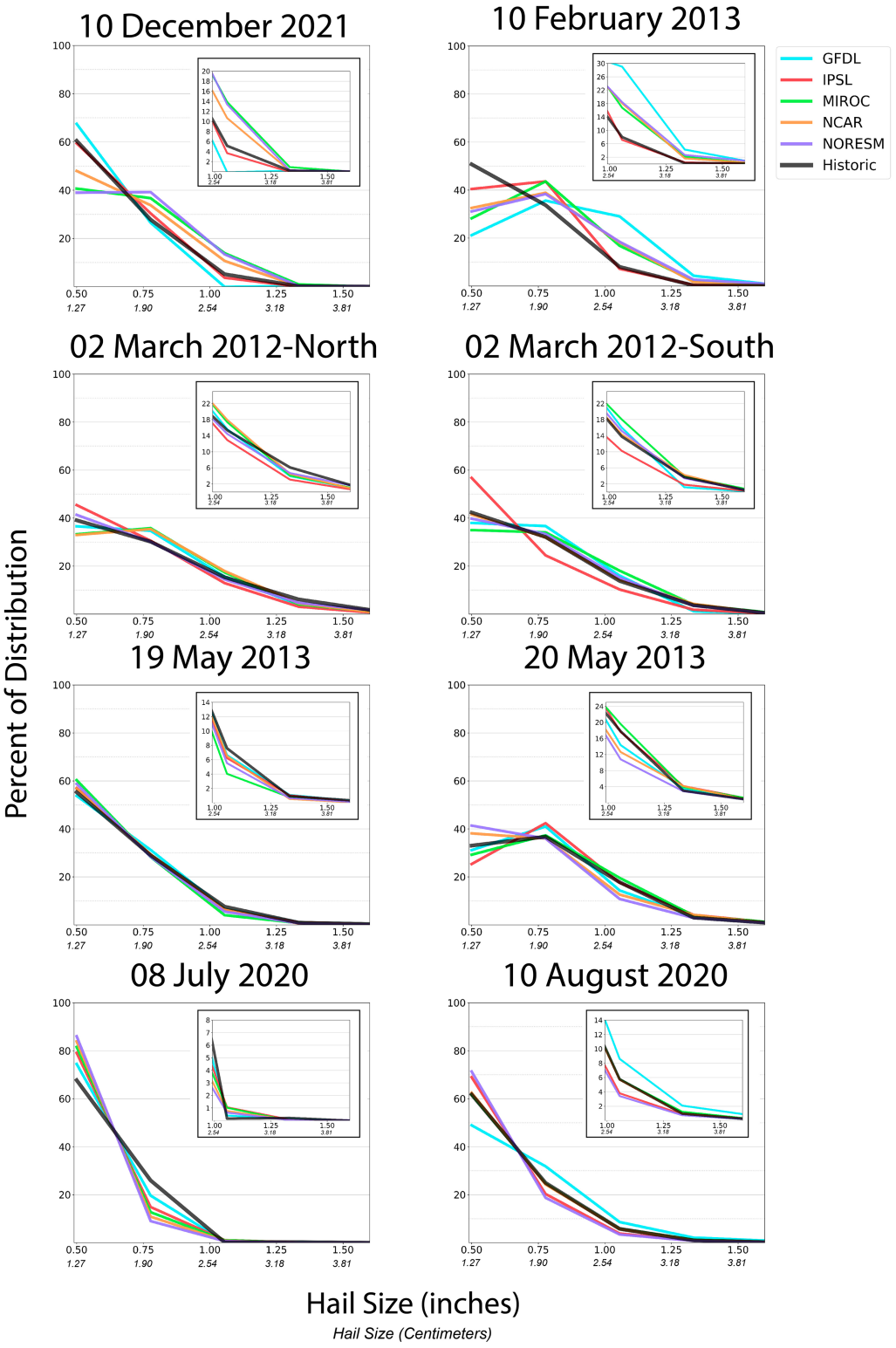

FIG. 9. As in Fig. 8, but showing distributions of column-maximum hail sizes over the entire simulation for each event. Insets show the distribution for hail diameters 1.0 in. (2.5 cm) and greater. There were no statistically significant changes for any events.

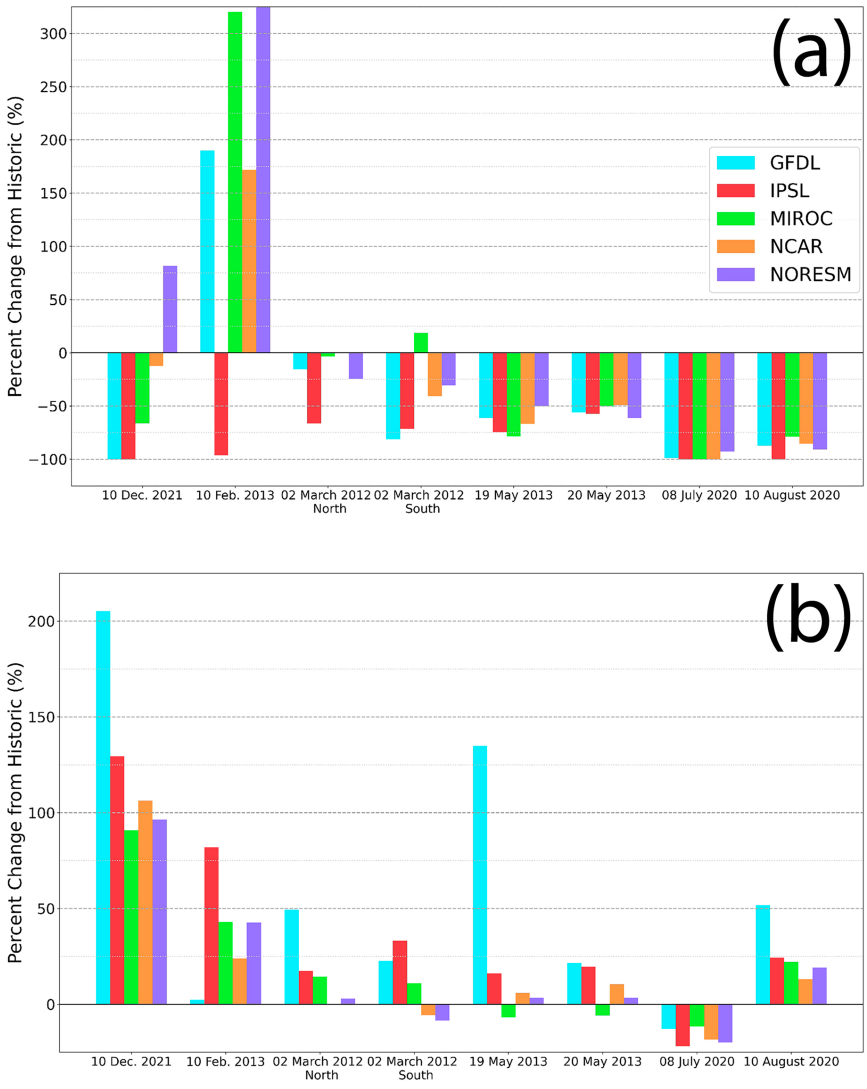

FIG. 10. (a) Percent change from HIST for the area of accumulated surface hailfall ≥ 1 mm normalized by total storm area for each event. The percentage value for the 10 Feb 2013 NORESM case is 667%. (b) Percent change from HIST for the area of accumulated surface rainfall area ≥ 0.01 in normalized by total storm area for each event.

the 95th percentile of the hail sizes at the surface for each simulation only varies by about ±0.15 in. (0.38 cm) between the HIST and PGW simulations within each event (Table 3). This is not unexpected given that the increases in the 95th percentile of updraft speeds are less than 5 m s^{-1} for nearly all PGW simulations (Table 2). While it is likely that the increases in updraft speeds for cold-season events contribute to increases in the amount of larger hail sizes at the surface, there is no clear distinction between the changes in cold-season versus warm-season updraft strengths that would indicate this is the primary cause of changes in the distribution of hail sizes.

An investigation of the distribution of maximum hail sizes in any grid column *above* the ground (supplied by the WRF output variable "HAIL_MAX2D") throughout each simulation (Fig. 9) helps to assess if the trends in the maximum hail sizes at the surface are related to the maximum hail sizes produced within the storms. Trends in the maximum hail sizes aloft mirror those at the surface (Fig. 8), with cold-season events generally showing an increase in maximum hail sizes within the storms, and warm-season events showing a decrease. There are no statistically significant changes in maximum hail sizes in the grid columns between the HIST and PGW simulations, for any events. Despite the warm-season events (barring 8 July 2020) having modestly stronger updrafts in the PGW simulations, larger hail is not produced within those storms.

4) MELTING DEPTH AND INFLUENCE ON RAINFALL

Despite a unanimous increase in hail melting depths across all the PGW environments for all events (Fig. 2e), it does not appear that this is the primary cause for the shift to smaller hail

sizes in the PGW warm-season storms, given the similar decreases in the maximum hail sizes both aloft and at the surface.

The increase in melting depth does, however, seem to impact changes in the area of hailfall accumulation (here defined as the area over which the WRF variable "HAILNC" exceeded 1 mm) when normalized by the total storm area for each simulation. For all events except 10 February 2013, a decrease in the area of hailfall accumulation occurs in the PGW simulations relative to the HIST simulations (Fig. 10a). The relatively smaller increase in melting depth (Fig. 2e) combined with a higher frequency of the larger hail sizes at the surface for the 10 February 2013 event, as compared to the other events, likely cause the increases seen in Fig. 10a.

Increases in hail melting also have implications for surface rainfall. Figure 10b shows the change in rainfall area between the HIST and PGW simulations for each event, using the WRF output variable RAINNC to compute the area of rainfall accumulations exceeding 0.01 mm when normalized by the total storm area. Most PGW simulations generally produce a larger area of rainfall, except for the 8 July 2020 case. However, the PGW simulations for the 10 February 2013 event have a larger area of rainfall as well, even though it also has a larger area of hailfall accumulation (Fig. 10a). Thus, the relationship between hail melting and rainfall accumulation is not as clear as one might expect. However, for the warm-season events (all except the December and February events), increased hail melting could be directly contributing to increases in rainfall. When the linear correlation is evaluated between the sum of hourly values of total hail mass in updrafts exceeding 10 m s^{-1} and either (i) event-total hailfall mass at the ground, or (ii) event-total rainfall mass at the ground, the correlation between hail mass in the updrafts and rainfall mass at the ground is much greater (Table 4).

The generally higher correlation between hail mass in the storm updrafts and rain mass at the surface, as one moves from cold-season to warm-season events, can be attributed to the shift to smaller hail sizes aloft in warm-season PGW storms paired with increases in melting depth, resulting in more rain at the surface. The relationship is not as strong in cold-season storms where hail sizes are larger aloft and less prone to melting completely, but hailstone shedding during growth (e.g., Miller et al. 1988) may be contributing to some of the increased rain mass for these events and thus obfuscating the melting effects. The best correlation for hail mass within the storm and at the ground occurs for the 8 July 2020 event, where *decreases* occur for both quantities as a result of weaker updrafts in the PGW storms, as discussed earlier.

Changes in the actual accumulated rainfall amounts across the domain for each event (using the "RAINNC" variable output by the WRF Model) show no clear trend between the HIST and PGW simulations (Fig. 11). Of those PGW storm events that do show statistically significant changes, the majority are related to a shift toward lower rainfall accumulations.

TABLE 4. Pearson correlation coefficients between total hail mass in storm updrafts and total rainfall or hailfall mass at the surface.

	Rainfall mass	Hailfall mass
10 Dec 2021	0.24	0.39
10 Feb 2013	0.52	0.54
2 Mar 2012–North	0.49	0.10
2 Mar 2012–South	0.58	0.60
19 May 2013	0.67	0.18
20 May 2013	0.89	−0.51
8 Jul 2020	0.92	0.85
10 Aug 2020	0.8	0.20

4. Conclusions and discussion

This study investigated the potential influences of a warmer end-of-century climate on changes in hail characteristics using the event-level pseudo–global warming (PGW) approach applied to seven historical hailstorm events over the United States that varied in intensity, geographical location, and season. These seven hailstorm events were first simulated using the WRF Model in their respective historical environments (HIST simulations) and then simulated again in five different PGW environments for each event (PGW simulations). The PGW environments were obtained from five different CMIP5 members run under the RCP8.5 scenario. This study thus considers climate projections from more GCMs than previous dynamical downscaling studies investigating hailstorm changes under anthropogenic climate change. Changes in large-scale environmental parameters evaluated from these GCM projections were found to be consistent with prior studies, generally showing increases in CAPE, CIN, precipitable water, and melting-level heights, and only small changes in vertical wind shear.

PGW storms had modestly stronger storm updrafts for the entire simulation; increases in the effects of entrainment due to those environments containing lower humidity air from 900 to 700 hPa, as well as increases in hydrometeor loading, may have prevented the realization of the strengths expected from increases in CAPE in the PGW environments. Despite modest increases in the updrafts in the PGW storms, only the cold-season events showed an increase in hail sizes both within the storms and at the ground. The warm-season events produced smaller hail both within the storms and at the ground. Changes in the hailfall area at the ground also showed a seasonal trend, with increases in cold-season events and decreases in warm-season events. Increased melting depths in the warm-season PGW environments likely contributed to greater rainfall from the PGW storms, particularly because of the increase in smaller hail within those storms that would be more susceptible to melting. However, there was no clear trend to suggest that increased hailfall was a significant contributor to higher rainfall accumulations in the simulations.

The ability to assess changes in hailfall and rainfall area is unique to the event-level PGW method given the ability to analyze detailed, high-resolution simulations of small spatiotemporal events. These results suggest that future hailstorms could potentially produce larger areas of rainfall (and in cold-season events, larger areas of hailfall as well) for a given amount of storm areal coverage, suggesting that the future risk of hailfall may only increase locally. Expectations from

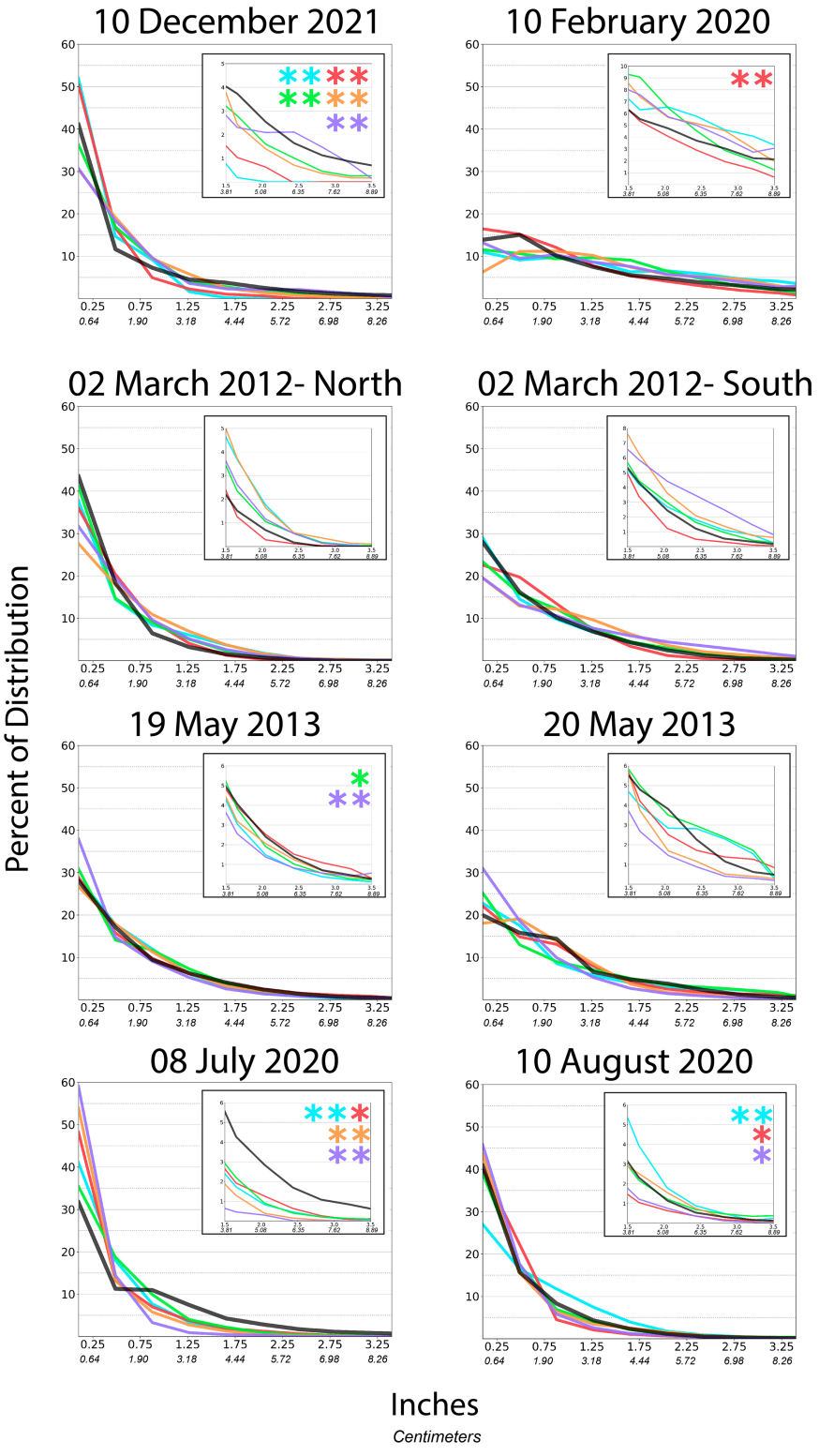

FIG. 11. Distribution of accumulated rainfall amounts for the simulated domain for each event. Insets for each event show the distribution for rainfall amounts 1.5 in. (3.8 cm) and greater. Statistically significant changes (based on a Mann–Whitney *U* test) at the 90% (95%) confidence interval are denoted by * (**).

prior studies (particularly those summarized in Table 1) were that increases in CAPE would lead to stronger updrafts that could support larger hail. This study found that this is (at least partially) true for cold-season events, where larger hail sizes were seen both aloft and at the surface. However, for warm-season storms, smaller hail sizes were seen both aloft and at the surface, precluding the role of increased melting depths in the future being the main factor in altering the hail size distribution at the ground in those cases.

Limitations to the current event-level PGW study are still inevitable, largely due to the associated computational cost. Even with using a larger number of events and predictions from GCMs compared to prior PGW studies, an adequate sample size is lacking to test the generality of these results. Thus, future studies should weigh these and other limitations against the benefits of this approach. In this regard, it is worthwhile to continue investigating linkages between the large-scale environment, storm kinematics, and hazards with other methods.

The deltas in this study were constructed using the RCP8.5 scenario at the end of the century to elicit the most extreme environmental response to ACC. Future work could utilize lower emissions scenarios and/or midcentury projections to gauge the response of hailstorms to these environments; doing so would also contribute to the growing body of work aimed at linking the large-scale environment to convective storm hazards and has implications for storm predictability and forecasting. Additionally, the monthly averaged deltas used here may not capture the more extreme environments that could occur on individual days and may be too conservative in their representation of a future environment.

While not unique to this study, there is uncertainty stemming from the representation of microphysical processes within numerical models. Model microphysics schemes use rate equations to represent processes acting on hydrometeors (i.e., evaporation of raindrops), but these rate equations are poorly constrained, especially for processes relating to ice-type hydrometeors (e.g., Morrison et al. 2020b). The use of a single microphysics scheme in the current study allows for a framework that at least keeps biases and uncertainties consistent across all simulations, to focus on how ACC influences storm processes.

Clearly, unanswered questions regarding the dominant influence in future changes in hailfall remain. As stated in Raupach et al. (2021), process-oriented studies are needed to investigate changes in the microphysical processes associated with hail production. In addition to helping understand how climate change will influence hail, such studies may help bridge the gap between environmental conditions and hail properties. To this end, the PGW methodology is well suited for such studies given the use of high-resolution simulations. The current study focused on environmental and mesoscale processes, but this was insufficient to explain the seasonal changes in hail sizes seen here. As noted in Dennis and Kumjian (2017), a number of microphysical processes must act in tandem with storm kinematics (e.g., a balance between hailstone size and updraft speed to suspend them) for optimal hail growth to occur. Competition among hailstones growing in storm updrafts, as well as changes in updraft area/hail growth volume can lead to changes in overall hail size as well. A more detailed study on changes in microphysical processes is warranted (and is underway, using these same simulations) to further evaluate how and why hail might change due to ACC.

Acknowledgments. All simulations were run on NCAR's Cheyenne supercomputer (https://doi.org/10.5065/D6RX99HX) and the authors would like to acknowledge the high-performance computing support provided by NCAR's Computational and Information Systems Laboratory, sponsored by the National Science Foundation. This work was supported by the National Science Foundation, Award AGS-1923042. The authors would also like to thank Dr. Kelly Mahoney for her input during the early stages of this work. Additionally, the authors thank the editor, Dr. Seung-Ki Min, as well as two anonymous reviewers for their time and recommendations on the manuscript, which undoubtedly improved it.

Data availability statement. GCM data were obtained from the Earth System Grid Federation, available at https://esgf-node.llnl.gov/projects/cmip5/. The HRRR data for this event are available at https://home.chpc.utah.edu/~u0553130/Brian_Blaylock/cgi-bin/hrrr_download.cgi. The NAM data for this event are available at https://www.ncei.noaa.gov/products/weather-climate-models/north-american-mesoscale. The WRF Model is open-source and can be downloaded at https://www2.mmm.ucar.edu/wrf/users/download/get_source.html. Both WRF-Python and MetPy are open-source Python packages and can be downloaded at https://wrf-python.readthedocs.io/en/latest/ and https://unidata.github.io/MetPy/latest/index.html, respectively.

REFERENCES

Allen, J. T., and M. K. Tippett, 2015: The characteristics of United States hail reports: 1955–2014. *Electron. J. Severe Storms Meteor.*, **10** (3), https://ejssm.com/ojs/index.php/site/article/view/60.

——, ——, Y. Kaheil, A. H. Sobel, C. Lepore, S. Nong, and A. Muehlbauer, 2017: An extreme value model for U.S. hail size. *Mon. Wea. Rev.*, **145**, 4501–4519, https://doi.org/10.1175/MWR-D-17-0119.1.

——, and Coauthors, 2020: Understanding hail in the Earth system *Rev. Geophys.*, **58**, e2019RG000665, https://doi.org/10.1029/2019RG000665.

Ashley, W. S., A. M. Haberlie, and V. A. Gensini, 2023: The future of supercells in the United States. *Bull. Amer. Meteor. Soc.*, **104**, E1–E21, https://doi.org/10.1175/BAMS-D-22-0027.1.

Blair, S. F., and J. W. Leighton, 2012: Creating high-resolution hail datasets using social media and post-storm ground surveys. *Electron. J. Oper. Meteor.*, **13**, 32–45.

——, and Coauthors, 2017: High-resolution hail observations: Implications for NWS warning operations. *Wea. Forecasting*, **32**, 1101–1119, https://doi.org/10.1175/WAF-D-16-0203.1.

Brimelow, J. C., G. W. Reuter, and E. R. Poolman, 2002: Modeling maximum hail size in Alberta thunderstorms. *Wea. Forecasting*, **17**, 1048–1062, https://doi.org/10.1175/1520-0434(2002)017<1048:MMHSIA>2.0.CO;2.

——, W. R. Burrows, and J. M. Hanesiak, 2017: The changing hail threat over North America in response to anthropogenic

climate change. *Nat. Climate Change*, **7**, 516–522, https://doi.org/10.1038/nclimate3321.

Brooks, H. E., 2013: Severe thunderstorms and climate change. *Atmos. Res.*, **123**, 129–138, https://doi.org/10.1016/j.atmosres.2012.04.002.

——, J. W. Lee, and J. P. Craven, 2003: The spatial distribution of severe thunderstorm and tornado environments from global reanalysis data. *Atmos. Res.*, **67–68**, 73–94, https://doi.org/10.1016/S0169-8095(03)00045-0.

Bryan, G. H., and H. Morrison, 2012: Sensitivity of a simulated squall line to horizontal resolution and parameterization of microphysics. *Mon. Wea. Rev.*, **140**, 202–225, https://doi.org/10.1175/MWR-D-11-00046.1.

Caine, S., T. P. Lane, P. T. May, C. Jakob, S. T. Siems, M. J. Manton, and J. Pinto, 2013: Statistical assessment of tropical convection-permitting model simulations using a cell-tracking algorithm. *Mon. Wea. Rev.*, **141**, 557–581, https://doi.org/10.1175/MWR-D-11-00274.1.

Cecil, D. J., 2009: Passive microwave brightness temperatures as proxies for hailstorms. *J. Appl. Meteor. Climatol.*, **48**, 1281–1286, https://doi.org/10.1175/2009JAMC2125.1.

Cintineo, J. L., T. M. Smith, V. Lakshmanan, H. E. Brooks, and K. L. Ortega, 2012: An objective high-resolution hail climatology of the contiguous United States. *Wea. Forecasting*, **27**, 1235–1248, https://doi.org/10.1175/WAF-D-11-00151.1.

Dawson, D. T., II, M. Xue, J. A. Milbrandt, and M. K. Yau, 2010: Comparison of evaporation and cold pool development between single-moment and multimoment bulk microphysics schemes in idealized simulations of tornadic thunderstorms. *Mon. Wea. Rev.*, **138**, 1152–1171, https://doi.org/10.1175/2009MWR2956.1.

Del Genio, A. D., M.-S. Yao, and J. Jonas, 2007: Will moist convection be stronger in a warmer climate? *Geophys. Res. Lett.*, **34**, L16703, https://doi.org/10.1029/2007GL030525.

Deng, A., and D. R. Stauffer, 2006: On improving 4-km mesoscale model simulations. *J. Appl. Meteor. Climatol.*, **45**, 361–381, https://doi.org/10.1175/JAM2341.1.

Dennis, E. J., and M. R. Kumjian, 2017: The impact of vertical wind shear on hail growth in simulated supercells. *J. Atmos. Sci.*, **74**, 641–663, https://doi.org/10.1175/JAS-D-16-0066.1.

Dessens, J., C. Berthet, and J. L. Sanchez, 2015: Change in hailstone size distributions with an increase in the melting level height. *Atmos. Res.*, **158–159**, 245–253, https://doi.org/10.1016/j.atmosres.2014.07.004.

Diffenbaugh, N. S., M. Scherer, and R. J. Trapp, 2013: Robust increases in severe thunderstorm environments in response to greenhouse forcing. *Proc. Natl. Acad. Sci. USA*, **110**, 16 361–16 366, https://doi.org/10.1073/pnas.1307758110.

Doswell, C. A., III, H. E. Brooks, and M. P. Kay, 2005: Climatological estimates of daily local nontornadic severe thunderstorm probability for the United States. *Wea. Forecasting*, **20**, 577–595, https://doi.org/10.1175/WAF866.1.

Edwards, R., and R. L. Thompson, 1998: Nationwide comparisons of hail size with WSR-88D vertically integrated liquid water and derived thermodynamic sounding data. *Wea. Forecasting*, **13**, 277–285, https://doi.org/10.1175/1520-0434(1998)013<0277:NCOHSW>2.0.CO;2.

Frei, C., C. Schär, D. Lüthi, and H. C. Davies, 1998: Heavy precipitation processes in a warmer climate. *Geophys. Res. Lett.*, **25**, 1431–1434, https://doi.org/10.1029/98GL51099.

Gensini, V. A., and T. L. Mote, 2014: Estimations of hazardous convective weather in the United States using dynamical downscaling. *J. Climate*, **27**, 6581–6589, https://doi.org/10.1175/JCLI-D-13-00777.1.

——, and ——, 2015: Downscaled estimates of late 21st century severe weather from CCSM3. *Climatic Change*, **129**, 307–321, https://doi.org/10.1007/s10584-014-1320-z.

——, C. Converse, W. S. Ashley, and M. Taszarek, 2021: Machine learning classification of significant tornadoes and hail in the United States using ERA5 proximity soundings. *Wea. Forecasting*, **36**, 2143–2160, https://doi.org/10.1175/WAF-D-21-0056.1.

Grabowski, W. W., and H. Morrison, 2020: Do ultrafine cloud condensation nuclei invigorate deep convection? *J. Atmos. Sci.*, **77**, 2567–2583, https://doi.org/10.1175/JAS-D-20-0012.1.

Haberlie, A. M., W. S. Ashley, C. M. Battisto, and V. A. Gensini, 2022: Thunderstorm activity under intermediate and extreme climate change scenarios. *Geophys. Res. Lett.*, **49**, e2022GL098779, https://doi.org/10.1029/2022GL098779.

Heymsfield, A., M. Szakáll, A. Jost, I. Giammanco, and R. Wright, 2018: A comprehensive observational study of graupel and hail terminal velocity, mass flux, and kinetic energy. *J. Atmos. Sci.*, **75**, 3861–3885, https://doi.org/10.1175/JAS-D-18-0035.1.

Holton, J. R., 2004: *An Introduction to Dynamic Meteorology*. 4th ed. Academic Press, 535 pp.

Hoogewind, K. A., M. E. Baldwin, and R. J. Trapp, 2017: The impact of climate change on hazardous convective weather in the United States: Insight from high-resolution dynamical downscaling. *J. Climate*, **30**, 10 081–10 100, https://doi.org/10.1175/JCLI-D-16-0885.1.

Igel, A. L., M. R. Igel, and S. C. van den Heever, 2015: Make it a double? Sobering results from simulations using single-moment microphysics schemes. *J. Atmos. Sci.*, **72**, 910–925, https://doi.org/10.1175/JAS-D-14-0107.1.

IPCC, 2021: *Climate Change 2021: The Physical Science Basis*. Cambridge University Press, 2391 pp., https://doi.org/10.1017/9781009157896.

Janssen Schile, E. E., D. Wuebbles, S. Stevens, R. Trapp, and B. Jewett, 2019: A radar-based study of severe hail outbreaks over the contiguous United States for 2000–2011. *Int. Climatol.*, **39**, 278–291, https://doi.org/10.1002/joc.5805.

Jewell, R., and J. Brimelow, 2009: Evaluation of Alberta hail growth model using severe hail proximity soundings from the United States. *Wea. Forecasting*, **24**, 1592–1609, https://doi.org/10.1175/2009WAF2222230.1.

Jiang, Z., M. R. Kumjian, R. S. Schrom, I. Giammanco, T. Brown-Giammanco, H. Estes, R. Maiden, and A. J. Heymsfield, 2019: Comparisons of electromagnetic scattering properties of real hailstones and spheroids. *J. Appl. Meteor. Climatol.*, **58**, 93–112, https://doi.org/10.1175/JAMC-D-17-0344.1.

Jo, E., and S. Lasher-Trapp, 2023: Entrainment in a simulated supercell thunderstorm. Part III: The influence of decreased environmental humidity and general effects upon precipitation efficiency. *J. Atmos. Sci.*, **80**, 1107–1122, https://doi.org/10.1175/JAS-D-22-0168.1.

Johnson, A. W., and K. E. Sugden, 2014: Evaluation of sounding-derived thermodynamic and wind-related parameters associated with large hail events. *Electron. J. Severe Storms Meteor.*, **9** (5), https://ejssm.com/ojs/index.php/site/article/view/57.

Kendon, E. J., and Coauthors, 2017: Do convection-permitting regional climate models improve projections of future precipitation change? *Bull. Amer. Meteor. Soc.*, **98**, 79–93, https://doi.org/10.1175/BAMS-D-15-0004.1.

Kimura, F., and A. Kitoh, 2007: Downscaling by pseudo global warming method. Final Rep. to the ICCAP, 4 pp., https://www.chikyu.ac.jp/P-C09/ICCAP/ICCAP_Final_Report/2/4-climate_kimura.pdf.

Knight, N. C., 1986: Hailstone shape factor and its relation to radar interpretation of hail. *J. Appl. Meteor. Climatol.*, **25**, 1956–1958, https://doi.org/10.1175/1520-0450(1986)025<1956:HSFAIR>2.0.CO;2.

Kunkel, K. E., and Coauthors, 2013: Monitoring and understanding trends in extreme storms: State of knowledge. *Bull. Amer. Meteor. Soc.*, **94**, 499–514, https://doi.org/10.1175/BAMS-D-11-00262.1.

Lackmann, G. M., 2013: The South-Central U.S. flood of May 2010: Present and future. *J. Climate*, **26**, 4688–4709, https://doi.org/10.1175/JCLI-D-12-00392.1.

——, 2015: Hurricane Sandy before 1900 and after 2100. *Bull. Amer. Meteor. Soc.*, **96**, 547–560, https://doi.org/10.1175/BAMS-D-14-00123.1.

Ladwig, W., 2017: Wrf-python, version 1.3.2. UCAR/NCAR, accessed 3 December 2022, https://doi.org/10.5065/D6W094P1.

Lamb, D., and J. Verlinde, 2011: *Physics and Chemistry of Clouds*. 1st ed. Cambridge University Press, 584 pp.

Lasher-Trapp, S., S. A. Orendorf, and R. J. Trapp, 2023: Investigating a derecho in a future warmer climate. *Bull. Amer. Meteor. Soc.*, **104**, E1831–E1852, https://doi.org/10.1175/BAMS-D-22-0173.1.

Lee, S. S., and L. J. Donner, 2011: Effects of cloud parameterization on radiation and precipitation: A comparison between single-moment microphysics and double-moment microphysics. *Terr. Atmos. Ocean. Sci.*, **22**, 403–420, https://doi.org/10.3319/TAO.2011.03.03.01(A).

Lepore, C., R. Abernathey, N. Henderson, J. T. Allen, and M. K. Tippett, 2021: Future global convective environments in CMIP6 models. *Earth's Future*, **9**, e2021EF002277, https://doi.org/10.1029/2021EF002277.

Li, M., F. Zhang, Q. Zhang, J. Y. Harrington, and M. R. Kumjian, 2017: Nonlinear response of hail precipitation rate to environmental moisture content: A real case modeling study of an episodic midlatitude severe convective event. *J. Geophys. Res. Atmos.*, **122**, 6729–6747, https://doi.org/10.1002/2016JD026373.

Lin, Y., and M. R. Kumjian, 2022: Influences of CAPE on hail production in simulated supercell storms. *J. Atmos. Sci.*, **79**, 179–204, https://doi.org/10.1175/JAS-D-21-0054.1.

Lindley, T. T., and L. R. Lemon, 2007: Preliminary observations of weak three-body scatter spikes associated with low-end severe hail. *Electron. J. Severe Storms Meteor.*, **2** (3), https://ejssm.com/ojs/index.php/site/article/view/8.

Mahoney, K., M. A. Alexander, G. Thompson, J. J. Barsugli, and J. D. Scott, 2012: Changes in hail and flood risk in high-resolution simulations over Colorado's mountains. *Nat. Climate. Change*, **2**, 125–131, https://doi.org/10.1038/nclimate1344.

——, ——, J. D. Scott, and J. Barsugli, 2013: High-resolution downscaled simulations of warm-season extreme precipitation events in the Colorado Front Range under past and future climates. *J. Climate*, **26**, 8671–8689, https://doi.org/10.1175/JCLI-D-12-00744.1.

Mansell, E. R., C. L. Ziegler, and E. C. Bruning, 2010: Simulated electrification of a small thunderstorm with two-moment bulk microphysics. *J. Atmos. Sci.*, **67**, 171–194, https://doi.org/10.1175/2009JAS2965.1.

May, R. M., and Coauthors, 2022: MetPy: A meteorological python library for data analysis and visualization. *Bull. Amer. Meteor. Soc.*, **103**, E2273–E2284, https://doi.org/10.1175/BAMS-D-21-0125.1.

Milbrandt, J. A., and M. K. Yau, 2006: A multimoment bulk microphysics parameterization. Part IV: Sensitivity experiments. *J. Atmos. Sci.*, **63**, 3137–3159, https://doi.org/10.1175/JAS3817.1.

Miller, L. J., J. D. Tuttle, and C. A. Knight, 1988: Airflow and hail growth in a severe northern High Plains supercell. *J. Atmos. Sci.*, **45**, 736–762, https://doi.org/10.1175/1520-0469(1988)045<0736:AAHGIA>2.0.CO;2.

Morrison, H., G. Thompson, and V. Tatarskii, 2009: Impact of cloud microphysics on the development of trailing stratiform precipitation in a simulated squall line: Comparison of one- and two-moment schemes. *Mon. Wea. Rev.*, **137**, 991–1007, https://doi.org/10.1175/2008MWR2556.1.

——, J. M. Peters, A. C. Varble, W. M. Hannah, and S. E. Giangrande, 2020a: Thermal chains and entrainment in cumulus updrafts. Part I: Theoretical description. *J. Atmos. Sci.*, **77**, 3637–3660, https://doi.org/10.1175/JAS-D-19-0243.1.

——, and Coauthors, 2020b: Confronting the challenge of modeling cloud and precipitation microphysics. *J. Adv. Model. Earth Syst.*, **12**, e2019MS001689, https://doi.org/10.1029/2019MS001689.

NOAA NCEI, 2022: U.S. billion-dollar weather and climate disasters, 1980–present. NCEI, accessed 12 July 2022, https://doi.org/10.25921/stkw-7w73.

Ortega, K. L., 2018: Evaluating multi-radar, multi-sensor products for surface hail-fall diagnosis. *Electron. J. Severe Storms Meteor.*, **13** (1), https://ejssm.org/archives/wp-content/uploads/2021/09/vol13-1.pdf.

Patricola, C. M., and M. F. Wehner, 2018: Anthropogenic influences on major tropical cyclone events. *Nature*, **563**, 339–346, https://doi.org/10.1038/s41586-018-0673-2.

Peters, J. M., D. R. Chavas, C.-Y. Su, H. Morrison, and B. E. Coffer, 2023: An analytic formula for entraining CAPE in mid-latitude storm environments. *J. Atmos. Sci.*, **80**, 2165–2186, https://doi.org/10.1175/JAS-D-23-0003.1.

Pilguj, N., M. Taszarek, J. T. Allen, and K. A. Hoogewind, 2022: Are trends in convective parameters over the United States and Europe consistent between reanalyses and observations? *J. Climate*, **35**, 3605–3626, https://doi.org/10.1175/JCLI-D-21-0135.1.

Poujol, B., A. F. Prein, and A. J. Newman, 2020: Kilometer-scale modeling projects a tripling of Alaskan convective storms in future climate. *Climate Dyn.*, **55**, 3543–3564, https://doi.org/10.1007/s00382-020-05466-1.

Prein, A. F., C. Liu, K. Ikeda, S. B. Trier, R. M. Rasmussen, G. J. Holland, and M. P. Clark, 2017a: Increased rainfall volume from future convective storms in the US. *Nat. Climate Change*, **7**, 880–884, https://doi.org/10.1038/s41558-017-0007-7.

——, R. M. Rasmussen, K. Ikeda, C. Liu, M. P. Clark, and G. J. Holland, 2017b: The future intensification of hourly precipitation extremes. *Nat. Climate Change*, **7**, 48–52, https://doi.org/10.1038/nclimate3168.

Rasmussen, R. M., and A. J. Heymsfield, 1987: Melting and shedding of graupel and hail. Part I: Model physics. *J. Atmos. Sci.*, **44**, 2754–2763, https://doi.org/10.1175/1520-0469(1987)044<2754:MASOGA>2.0.CO;2.

——, and Coauthors, 2011: High-resolution coupled climate runoff simulations of seasonal snowfall over Colorado: A process study of current and warmer climate. *J. Climate*, **24**, 3015–3048, https://doi.org/10.1175/2010JCLI3985.1.

Raupach, T. H., and Coauthors, 2021: The effects of climate change on hailstorms. *Nat. Rev. Earth Environ.*, **2**, 213–226, https://doi.org/10.1038/s43017-020-00133-9.

Robinson, E. D., R. J. Trapp, and M. E. Baldwin, 2013: The geospatial and temporal distributions of severe thunderstorms from high-resolution dynamical downscaling. *J. Appl. Meteor. Climatol.*, **52**, 2147–2161, https://doi.org/10.1175/JAMC-D-12-0131.1.

Roh, W., and M. Satoh, 2014: Evaluation of precipitating hydrometeor parameterizations in a single-moment bulk microphysics scheme for deep convective systems over the tropical central Pacific. *J. Atmos. Sci.*, **71**, 2654–2673, https://doi.org/10.1175/JAS-D-13-0252.1.

Ryzhkov, A. V., M. R. Kumjian, S. M. Ganson, and A. P. Khain, 2013: Polarimetric radar characteristics of melting hail. Part I: Theoretical simulations using spectral microphysical modeling. *J. Appl. Meteor. Climatol.*, **52**, 2849–2870, https://doi.org/10.1175/JAMC-D-13-073.1.

Sato, T., F. Kimura, and A. Kitoh, 2007: Projection of global warming onto regional precipitation over Mongolia using a regional climate model. *J. Hydrol.*, **333**, 144–154, https://doi.org/10.1016/j.jhydrol.2006.07.023.

Schär, C., C. Frei, D. Lüthi, and H. C. Davies, 1996: Surrogate climate-change scenarios for regional climate models. *Geophys. Res. Lett.*, **23**, 669–672, https://doi.org/10.1029/96GL00265.

Seeley, J. T., and D. M. Romps, 2015: The effect of global warming on severe thunderstorms in the United States. *J. Climate*, **28**, 2443–2458, https://doi.org/10.1175/JCLI-D-14-00382.1.

Shedd, L., M. R. Kumjian, I. Giammanco, T. Brown-Giammanco, and B. R. Maiden, 2021: Hailstone shapes. *J. Atmos. Sci.*, **78**, 639–652, https://doi.org/10.1175/JAS-D-20-0250.1.

Skamarock, W. C., and Coauthors, 2019: A description of the Advanced Research WRF model version 4. NCAR Tech. Note NCAR/TN-556+STR, 145 pp., https://doi.org/10.5065/1dfh-6p97.

Tang, B. H., V. A. Gensini, and C. R. Homeyer, 2019: Trends in United States large hail environments and observations. *npj Climate Atmos. Sci.*, **2**, 45, https://doi.org/10.1038/s41612-019-0103-7.

Taszarek, M., J. T. Allen, H. E. Brooks, N. Pilguj, and B. Czernecki, 2021: Differing trends in United States and European severe thunderstorm environments in a warming climate. *Bull. Amer. Meteor. Soc.*, **102**, E296–E322, https://doi.org/10.1175/BAMS-D-20-0004.1.

Thompson, G., P. R. Field, R. M. Rasmussen, and W. D. Hall, 2008: Explicit forecasts of winter precipitation using an improved bulk microphysics scheme. Part II: Implementation of a new snow parameterization. *Mon. Wea. Rev.*, **136**, 5095–5115, https://doi.org/10.1175/2008MWR2387.1.

Trapp, R. J., and K. A. Hoogewind, 2016: The realization of extreme tornadic storm events under future anthropogenic climate change. *J. Climate*, **29**, 5251–5265, https://doi.org/10.1175/JCLI-D-15-0623.1.

——, N. S. Diffenbaugh, H. E. Brooks, M. E. Baldwin, E. D. Robinson, and J. S. Pal, 2007: Changes in severe thunderstorm environment frequency during the 21st century caused by anthropogenically enhanced global radiative forcing. *Proc. Natl. Acad. Sci. USA*, **104**, 19 719–19 723, https://doi.org/10.1073/pnas.0705494104.

——, E. D. Robinson, M. E. Baldwin, N. S. Diffenbaugh, and B. R. J. Schwedler, 2011: Regional climate of hazardous convective weather through high-resolution dynamical downscaling. *Climate Dyn.*, **37**, 677–688, https://doi.org/10.1007/s00382-010-0826-y.

——, K. A. Hoogewind, and S. Lasher-Trapp, 2019: Future changes in hail occurrence in the United States determined through convection-permitting dynamical downscaling. *J. Climate*, **32**, 5493–5509, https://doi.org/10.1175/JCLI-D-18-0740.1.

——, M. J. Woods, S. G. Lasher-Trapp, and M. A. Grover, 2021: Alternative implementations of the "pseudo-global-warming" methodology for event-based simulations. *J. Geophys. Res. Atmos.*, **126**, e2021JD035017, https://doi.org/10.1029/2021JD035017.

Van Klooster, S. L., and P. J. Roebber, 2009: Surface-based convective potential in the contiguous United States in a business-as-usual future climate. *J. Climate*, **22**, 3317–3330, https://doi.org/10.1175/2009JCLI2697.1.

Van Weverberg, K., A. M. Vogelmann, H. Morrison, and J. A. Milbrandt, 2012: Sensitivity of idealized squall-line simulations to the level of complexity used in two-moment bulk microphysics schemes. *Mon. Wea. Rev.*, **140**, 1883–1907, https://doi.org/10.1175/MWR-D-11-00120.1.

——, and Coauthors, 2013: The role of cloud microphysics parameterization in the simulation of mesoscale convective system clouds and precipitation in the tropical western Pacific. *J. Atmos. Sci.*, **70**, 1104–1128, https://doi.org/10.1175/JAS-D-12-0104.1.

Witt, A., M. D. Eilts, G. J. Stumpf, J. T. Johnson, E. D. Mitchell, and K. W. Thomas, 1998: An enhanced hail detection algorithm for the WSR-88D. *Wea. Forecasting*, **13**, 286–303, https://doi.org/10.1175/1520-0434(1998)013<0286:AEHDAF>2.0.CO;2.

Woods, M. J., R. J. Trapp, and H. M. Mallinson, 2023: The impact of human-induced climate change on future tornado intensity as revealed through multi-scale modeling. *Geophys. Res. Lett.*, **50**, e2023GL104796, https://doi.org/10.1029/2023GL104796.